A RELAXATION SCHEME FOR THE EQUATIONS OF ISENTROPIC GAS DYNAMICS ON A NETWORK WITH JUMP TRANSMISSION CONDITIONS

MAYA BRIANI, ROBERTO NATALINI, AND MAGALI RIBOT

Abstract. This paper addresses the numerical modeling of isentropic gas dynamics on one-dimensional networks, focusing on the Euler equations with a novel class of transmission conditions at network junctions, termed the Jump Transmission Condition (JTC). Unlike traditional models that enforce continuity of density at junctions, the (JTC) allows for a density jump proportional to the flux, reflecting phenomena such as bottlenecks in biological or traffic networks. The authors propose a relaxation scheme based on the vector BGK approach, which ensures mass conservation and enforces the (JTC) without requiring the explicit solution of the Riemann problem at the junction. The scheme is analyzed for its mathematical properties, including entropy dissipation and positivity, and is compared with classical solvers based on the explicit solution of the Riemann problem. Numerical experiments on simple and complex networks demonstrate the accuracy, robustness, and flexibility of the proposed method, especially in handling both subsonic and supersonic regimes and in extending to general networks.

1. Introduction

In this article, we consider the Euler equations of isentropic gas dynamics set on the one dimensional arcs of a network. On these arcs the Euler equations are, as usual, given by:

$$\begin{cases} \partial_t \rho + \partial_x(\rho u) = 0, \\ \partial_t(\rho u) + \partial_x(\rho u^2 + p(\rho)) = 0, \end{cases} \tag{1}$$

where x is a spatial coordinate, $t > 0$ is the time, ρ is the density of a fluid, so we will assume all the time $\rho > 0$, and $q = \rho u$ its momentum. Also, we shall assume that the pressure p is given by the pressure law for isentropic gases, that is to say

$$p(\rho) = p_0\ \rho^\gamma \text{ with } \gamma \geq 1. \tag{2}$$

Usually, for isentropic fluids, the value of γ is taken such that $1 \leq \gamma < 5/3$. However, here, we have in mind various applications, and in particular to biology, see for instance [31, 57, 53], where the value of γ can range in a larger interval, so in the following we consider all the values $\gamma \geq 1$.

While on the external boundary of the network we can assign, for instance, standard no-flux conditions to the gas, at the junction we have to impose some physically motivated transmission conditions. In this paper, we address a particular class of transmission conditions that, on a 2-arc network – i.e.: a network composed by just two arcs which meet at just one junction point, see Figure 1 – at the junction point x reads as:

$$(\rho u)_\ell(t, x_\ell) = (\rho u)_r(t, x_r) = \kappa(\rho_\ell(t, x_\ell) - \rho_r(t, x_r)), \text{ for all time } t > 0, \tag{3}$$

where the subscripts ℓ and r stand respectively for the left and right sides of the junction point and κ is a given positive constant. In the following we shall refer to these conditions as the Jump Transmission Condition (JTC). In fact, the first equality in (JTC) implies that the density flux incoming at the junction is equal to the one outgoing and so the total mass is conserved at the junction. This is similar to the Kirchoff's law for an electrical circuit. This feature is common to most of the models of flows based on gas dynamics on networks. However, the second equality in (JTC) says that the density has to jump at the junction, and the jump is proportional to the density flux.

This condition is in a sharp contrast with most of the current models of fluid on networks. Actually, besides the conservation of mass, almost all of these models impose a supplementary continuity condition at the junction, as for instance in [51, 24, 28, 60], both for parabolic and hyperbolic models, see also [32, 11] for some informed reviews in the hyperbolic case.

For instance, in the framework of gas dynamics, a quite common application is the modeling of high-pressure gas pipelines [5, 26, 41], where the typical ratio between the pipe length and the diameter justifies a one space dimension approximation. When multiple pipes are connected at a nodal point, suitable conditions of transmission have to be prescribed. So, in the case of a 2-arc network of pipes of different diameters, a first condition can be, with the previous notations,

$$a_\ell(\rho u)_\ell(t, x_\ell) = a_r(\rho u)_r(t, x_r), \tag{4}$$

which ensures the conservation of mass. Here a_ℓ and a_r are the surface sections respectively of the left and the right pipe. Since a second condition has to be imposed, a typical additional condition can be, for instance, to impose the equal pressure at the junction

$$p(\rho_\ell) = p(\rho_r), \tag{5}$$

or, otherwise, the continuity of the dynamic pressure at the junction

$$a_\ell \left((\rho_\ell u_\ell^2) + p(\rho_\ell)\right) = a_r \left((\rho_r u_r^2) + p(\rho_r)\right). \tag{6}$$

In a different context, the junction can host a compressor station for two pipes with the same section. In this case, the second condition becomes something like

$$\left(\frac{p(\rho_\ell)}{p(\rho_r)} - 1\right)^{(\gamma-1)/\gamma} = \Pi(t), \tag{7}$$

where $\Pi(t)$ is the power exerted by the compressor, see for instance [43]. Notice that, in this last example, the density of the gas is discontinuous, but the mechanism appears quite different from the model we deal with in the following, since the ratio of the pressures is fixed and does not depend on the flux.

In the similar case of networks of open canals [6, 16, 17, 18], or for blood flows [21, 49], condition (4) is supplemented with continuity conditions similar to (5) or (6).

It is in this second condition that the (JTC), given by (3), differs, since it prescribes a jump discontinuity of the density at the junction, which varies with the flux. The (JTC) is analogous to transmission conditions introduced, only for diffusive problems, in the simple case of two regions, by Kedem and Katchalsky in [47], as permeability conditions in the description of passive transport through a biological membrane, see also [55, 19, 20] for various mathematical and related formulations. For instance, consider the porous medium equation, for $p(\rho) = D\rho^\gamma$, with $\gamma \geq 1$:

$$\partial_t \rho - \partial_{xx} p(\rho) = 0.$$

In this case, the density flux is given by $q = -\partial_x p(\rho)$, and the Kedem-Katchalsky condition reads

$$-\partial_x p(\rho_\ell)(t, L_\ell) = -\partial_x p(\rho_r)(t, 0) = \kappa(\rho_\ell(t, L_\ell) - \rho_r(t, 0)), \tag{8}$$

as for instance in [23, 22], which are concerned with biological flows.

More recently, the Kedem-Katchalsky conditions were generalized to hyperbolic problems in the case of the linear Cattaneo equation and proposed as transmission conditions for hyperbolic-parabolic and hyperbolic-elliptic systems describing biological situations such as the movement of microorganisms on networks driven by chemotaxis. In the simplest case considered in the above papers, we have a linear wave equation

$$\begin{cases} \partial_t \rho + \partial_x q = 0, \\ \partial_t q + D\partial_x \rho = 0, \end{cases} \tag{9}$$

with $q = \rho u$ and, at the junction, with the same notations as before, we have

$$(\rho u)_\ell = (\rho u)_r = \kappa(\rho_\ell - \rho_r). \tag{10}$$

This condition has been introduced first in [14] to take into account the movement of fibroblasts on a network, and then studied in [36, 37, 38, 39, 40], see also [15, 12] for other models and the numerical treatment of these conditions in related situations.

In general, density jump conditions like (JTC) seem to be more appropriate than full continuity conditions when dealing with mathematical models for movements of individuals, as in traffic flows [33, 13, 34] or in biological phenomena involving bacteria, eukariotic cells, or other microorganism movements, as in [14, 36], where, even if the flux is continuous and the mass is conserved, discontinuities at the inner nodes for the density functions are expected, as a sort of mathematical counterpart of bottleneck phenomena. The reader can just imagine the flow of a crowd through a door: the mass is clearly conserved, but the density of people before and after the door can be very different. These previous conditions represent some transmission conditions through a jump (given by a membrane or a change of domain), and the fluxes are linked with the difference of densities on both sides of the jump.

To show that the (JTC) is the hyperbolic analogous of the parabolic Kedem-Katchalsky transmission condition, we can look at the diffusive limit of the damped version of equation (1), by scaling this equation as in [30], to obtain the perturbed system

$$\begin{cases} \partial_t \rho + \partial_x(\rho u) = 0, \\ \partial_t(\epsilon^2 \rho u) + \partial_x(\epsilon^2 \rho u^2 + p(\rho)) = -\rho u, \end{cases}$$

where the inertial terms $\partial_t(\rho u) + \partial_x(\rho u^2)$ are supposed to be negligible.

So, as ϵ tends to zero, the momentum ρu approaches $-\partial_x p(\rho)$ and, as shown in [30], we obtain the porous medium equation (1). Then, replacing $q = \rho u$ by $-\partial_x p(\rho)$ in (3), we obtain condition (8).

The purpose of this article is to propose a numerical scheme for system (1) on a network, with the (JTC) at each junction, based on the vector BGK approach [4, 10], which guarantees that condition (3) is fulfilled without solving the Riemann problem. Actually, we propose a way to solve the (JTC) relation with a scheme which also satisfies a momentum equality junction condition, namely the fact that at the discrete level the equality of the momenta $q = \rho u$ will be enforced both as the unknown of the second equation of system (1) and as the flux of the first equation of system (1).

This approach, as long as it is possible, will be compared with a more classical solver based on the Riemann invariants at the junction, which in the following will be referred as "Riemann invariant junction condition". Unfortunately, as we will discuss in this paper, it is not clear how to deal with this approach in the general "non-subsonic" case, so the comparison will be restricted to the situations where both approaches work.

The article is organized as follows : in Section 2 we study the mathematical formulation of equations (1) on a 2-arc network, with the conditions (3) at the junction and we show that the entropy is dissipated at least for situations where the density jump is small at the junction. In Section 3, we study how to solve the Riemann problem for (1) on a 2-arc network, with the conditions (3) at the junction using the classical approach with the Riemann invariants. We are able to find a solution in the subsonic case, and for some special initial conditions in the supersonic case. This is the first study of this problem in the literature.

Then, in Section 4, we introduce our relaxation scheme for the same problem, which can be written for all initial data. In Section 5, we present many numerical tests, and in particular a comparison between the relaxation scheme and the cases where we have an explicit solution for the Riemann problem at the junction. Finally we extend the previous study to the case of a general network in Section 6.

2. Isentropic gas dynamics on a 2-arc network: some basic properties

Consider now the 1D system (1) on a simple network, composed of two arcs, as displayed in Figure 1. The quantities linked to the arc on the left, called arc ℓ (resp. on the right, called arc r) are denoted with subscript ℓ (resp. r).

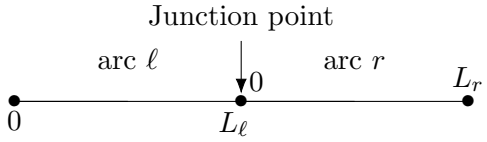

Figure 1. The 2-arc network : the quantities linked to the arc $[0, L_\ell]$ on the left (resp. $[0, L_r]$ on the right) are denoted with subscript ℓ (resp. r).

We are therefore dealing with the two following systems :

$$\begin{cases} \partial_t \rho_\ell(t,x) + \partial_x(\rho_\ell u_\ell)(t,x) = 0, \\ \partial_t(\rho_\ell u_\ell)(t,x) + \partial_x(\rho_\ell u_\ell^2 + p(\rho_\ell))(t,x) = 0, \end{cases} \quad \text{for } x \in [0, L_\ell], \tag{11}$$

and

$$\begin{cases} \partial_t \rho_r(t,x) + \partial_x(\rho_r u_r)(t,x) = 0, \\ \partial_t(\rho_r u_r)(t,x) + \partial_x(\rho_r u_r^2 + p(\rho_r))(t,x) = 0, \end{cases} \quad \text{for } x \in [0, L_r], \tag{12}$$

complemented with no-flux boundary conditions, at least for smooth solutions, at the external points of the two intervals, namely, always setting for the flux $q = \rho u$ in the following :

$$\begin{cases} \partial_x \rho_\ell(t,0) = 0, \quad q_\ell(t,0) = 0, \text{ for all } t \geq 0 \text{ on the left arc}, \\ \partial_x \rho_r(t,L_r) = 0, \quad q_r(t,L_r) = 0, \text{ for all } t \geq 0 \text{ on the right arc}. \end{cases} \tag{13}$$

Clearly the boundary conditions, as usual for hyperbolic problems, have to be intended in a proper sense, since sometimes, due to the direction of the characteristics with respect to the boundary, they need to be interpreted, see [59] and references therein for more details.

Finally, we define transmission conditions at the junction, which couple the unknowns of both systems. We want to ensure the mass conservation of the system, that is to says :

$$\frac{d}{dt}m(t) = 0, \text{ with } m(t) = \int_0^{L_\ell} \rho_\ell(t,x)\,dx + \int_0^{L_r} \rho_r(t,x)\,dx. \tag{14}$$

For that purpose, working with smooth solution and using condition (13), we have to consider the equality of fluxes at the junction :

$$q_\ell(t, L_\ell) = q_r(t, 0), \text{ for all } t \geq 0. \tag{15}$$

Now, we supplement this condition with a jump transmission condition (JTC) for the density at the junction, that is to say :

$$q_\ell(t, L_\ell) = q_r(t, 0) = \kappa(\rho_\ell(t, L_\ell) - \rho_r(t, 0)), \text{ for all } t \geq 0, \tag{16}$$

where κ is a *permeability coefficient* that we suppose to be constant.

Let us prove now that, at least for smooth solutions and in the case where $\gamma > 1$, system (11)-(3) is endowed with an entropy dissipation property at the continuous level under the condition that the density jump is small enough at the junction.

First, on an interval, there exists at least an entropy–entropy flux pair (η, G) for system (1), see [29] p.212, namely the functions

$$\eta(\rho, \rho u) = \frac{1}{2}\rho u^2 + \frac{p_0}{\gamma - 1}\rho^\gamma \text{ and } G(\rho, \rho u) = \left(\frac{1}{2}\rho u^2 + \frac{p_0\gamma}{\gamma - 1}\rho^\gamma\right) u \tag{17}$$

defined for $\gamma > 1$.

The function η is convex and, for smooth solutions $(\rho, q = \rho u)$ to system (1) we have

$$\partial_t \eta(\rho, q) + \partial_x G(\rho, q) = 0.$$

For weak solutions, the admissible (entropy) solutions have to verify (in the weak sense) the inequality

$$\partial_t \eta(\rho, q) + \partial_x G(\rho, q) \leq 0, \tag{18}$$

and we can say that the admissible solutions dissipate the entropy (see again [29]). In general, for one single interval $[0, L]$ with no flux conditions, the quantity

$$\int_0^L \eta(\rho(t,x), q(t,x))dx$$

is decreasing in time.

Now, we want to investigate if condition (JTC) in (3) preserves this dissipation property, at least in some range of solutions. Let us consider smooth solutions to equation (18) on the 2

arcs of the previous network and integrate it with respect to time and space :

$$\begin{aligned} S(t) &:= \int_0^{L_\ell} \eta(\rho_\ell(t,x), q_\ell(t,x))dx + \int_0^{L_r} \eta(\rho_r(t,x), q_r(t,x))dx \\ &\leq \int_0^{L_\ell} \eta(\rho_\ell(0,x), q_\ell(0,x))dx + \int_0^{L_r} \eta(\rho_r(0,x), q_r(0,x))dx \\ &- \int_0^t \left(G(\rho_\ell(s,L_\ell), q_\ell(s,L_\ell)) - G(\rho_\ell(s,0), q_\ell(s,0))\right) ds \\ &- \int_0^t \left(G(\rho_r(s,L_r), q_r(s,L_r)) - G(\rho_r(s,0), q_r(s,0))\right) ds. \end{aligned}$$

Thanks to boundary conditions on the external domain, we find that since $\gamma > 1$, we have

$$G(\rho_r(s,L_r), q_r(s,L_r)) = G(\rho_\ell(s,0), q_\ell(s,0)) = 0,$$

which leads to the inequality :

$$\begin{aligned} S(t) &= \int_0^{L_\ell} \eta(\rho_\ell(t,x), q_\ell(t,x))dx + \int_0^{L_r} \eta(\rho_r(t,x), q_r(t,x))dx \\ &\leq \int_0^{L_\ell} \eta(\rho_\ell(0,x), q_\ell(0,x))dx + \int_0^{L_r} \eta(\rho_r(0,x), q_r(0,x))dx \\ &- \int_0^t \left(G(\rho_\ell(s,L_\ell), q_\ell(s,L_\ell)) - G(\rho_r(s,0), q_r(s,0))\right) ds. \end{aligned} \tag{19}$$

Therefore, if the quantity $\Delta G(t) := G(\rho_\ell(t,L_\ell), q_\ell(t,L_\ell)) - G(\rho_r(t,0), q_r(t,0)) \geq 0$ for all $t > 0$, we have entropy dissipation, that is to say for all $t > 0$ it holds

$$S(t) \leq S(0).$$

Now, using the conditions at the junction, we can compute ΔG as follows. Using that $\rho > 0$, we rewrite $G(\rho, q)$ as :

$$G(\rho, q) = G(\rho, \rho u) = \frac{1}{2}\rho u^3 + \frac{p_0\gamma}{\gamma - 1}\rho^\gamma u = \frac{1}{2}\frac{q^3}{\rho^2} + \frac{p_0\gamma}{\gamma - 1}\rho^{\gamma-1} q$$

and therefore

$$\begin{aligned} &\Delta G(t) = G(\rho_\ell(t,L_\ell), q_\ell(t,L_\ell)) - G(\rho_r(t,0), q_r(t,0)) \\ &= \frac{1}{2}\left(\frac{(q_\ell(t,L_\ell))^3}{(\rho_\ell(t,L_\ell))^2} - \frac{(q_r(t,0))^3}{(\rho_r(t,0))^2}\right) + \frac{p_0\gamma}{\gamma - 1}\left((\rho_\ell(t,L_\ell))^{\gamma-1} q_\ell(t,L_\ell) - (\rho_r(t,0))^{\gamma-1} q_r(t,0)\right) \end{aligned}$$

Using the conditions (3) at the junction, the previous expression can be simplified as :

$$\begin{aligned} \Delta G(t) &= G(\rho_\ell(t,L_\ell), q_\ell(t,L_\ell)) - G(\rho_r(t,0), q_r(t,0)) \\ &= -\frac{1}{2}\kappa^3(\rho_\ell(t,L_\ell) - \rho_r(t,0))^4 \frac{\rho_r(t,0) + \rho_\ell(t,L_\ell)}{(\rho_r(t,0))^2(\rho_\ell(t,L_\ell))^2} \\ &\quad + \frac{p_0\gamma}{\gamma - 1}\kappa(\rho_\ell(t,L_\ell) - \rho_r(t,0))\left((\rho_\ell(t,L_\ell))^{\gamma-1} - (\rho_r(t,0))^{\gamma-1}\right). \end{aligned}$$

The first term on the right hand-side is negative whereas the second one is positive. We remark that as long as the difference $\rho_\ell(t,L_\ell) - \rho_r(t,0)$ is small,

$$\Delta G(t) \sim \frac{p_0\gamma}{\gamma - 1}\kappa(\rho_\ell(t,L_\ell) - \rho_r(t,0))\left((\rho_\ell(t,L_\ell))^{\gamma-1} - (\rho_r(t,0))^{\gamma-1}\right) \geq 0,$$

and the dissipation entropy property holds, whereas as the difference $\rho_\ell(t,L_\ell)-\rho_r(t,0)$ becomes large, we have

$$\Delta G(t) \sim -\frac{1}{2}\kappa^3(\rho_\ell(t,L_\ell)-\rho_r(t,0))^4\frac{\rho_r(t,0)+\rho_\ell(t,L_\ell)}{(\rho_r(t,0))^2(\rho_\ell(t,L_\ell))^2} \leq 0,$$

and then, a priori, the dissipation property is no longer true. In Section 5 we will test this dissipation property more closely, for various initial data, since in some cases the dissipation inside the arcs can compensate the growth of the entropy at the junction.

Remark 2.1. *Notice that, in the linear case of the wave equation* (9)*, the same dissipation was found in* [14] *by a simpler energy estimate. Actually, consider system* (9) *on the 2-arc network composed by the arc* $[0,L_\ell]$ *on the left (resp.* $[0,L_r]$ *on the right), with* $q_\ell(t,0)=q_r(t,L_r)=0$*. Multiply the first equation in* (9) *by* ρ *and the second by* q/D*, to get the energy equality*

$$\partial_t\left(\frac{1}{2}\rho^2+\frac{1}{2D}q^2\right)+\partial_x(\rho q)=0. \tag{20}$$

So, integrating on both $[0,L_\ell]$ *and* $[0,L_r]$*, we have that, thanks again to the no-flux conditions at the external nodes,*

$$\begin{aligned} S(t) &:= \int_0^{L_\ell}\left(\frac{1}{2}\rho_\ell^2+\frac{1}{2D}q_\ell^2\right)(t)dx+\int_0^{L_r}\left(\frac{1}{2}\rho_r^2+\frac{1}{2D}q_r^2\right)(t)dx \\ &= \int_0^{L_\ell}\left(\frac{1}{2}\rho_\ell^2+\frac{1}{2D}q_\ell^2\right)(0)dx+\int_0^{L_r}\left(\frac{1}{2}\rho_r^2+\frac{1}{2D}q_r^2\right)(0)dx \\ &\quad -\int_0^t(\rho_\ell q_\ell)(s,L_\ell)-(\rho_r q_r)(s,0)ds. \end{aligned}$$

So the energy of the system $S(t)$ *is dissipated if*

$$(\rho_\ell q_\ell)(s,L_\ell)-(\rho_r q_r)(s,0)\geq 0.$$

Now, if $q_\ell(s,L_\ell)=q_r(s,0)=q(s)$*, we have*

$$S(t)=S(0)-\int_0^t q(s)\left(\rho_\ell(s,L_\ell)-\rho_r(s,0)\right)ds, \tag{21}$$

So, the dissipation can occur in two different ways:

a) if $\rho_\ell(s,L_\ell)=\rho_r(s,0)$*, which is the standard continuity condition at the junction;*

b) if $q(s)=\kappa\left(\rho_\ell(s,L_\ell)-\rho_r(s,0)\right)$*, with* $\kappa>0$*, which is the present version of our condition* (3)*.*

A similar computation can be made for the case of the parabolic problem with Kedem-Katchalsky condition. So, in this sense, our (JTC) is the hyperbolic nonlinear generalization of these previous transmission conditions, and the natural one if we are not imposing the continuity of the density at the junction.

3. The Riemann problem at the junction - the case of a 2-arc network

We want to solve the Riemann problem for (11)–(3) at the junction using the classical approach with Riemann invariants.

3.1. **The Riemann problem on a single interval.** Let us first describe Riemann invariants on an interval before generalizing it to the junction case, see for example [29] for more details.

Let consider isentropic gas dynamics given by Eq.(1) on a single arc, under the form

$$\partial_t U + \partial_x F(U) = 0, \tag{22}$$

where $U \in \mathbb{R}^2$ is the vector of unknowns $U = \begin{pmatrix} \rho \\ q = \rho u \end{pmatrix}$, and the function $F : \mathbb{R}^2 \to \mathbb{R}^2$ is the flux of the system defined by $F(U) = \begin{pmatrix} \rho u \\ \rho u^2 + p(\rho) \end{pmatrix}$.

The eigenvalues of the system are

$$\mu_1(\rho, q) = \frac{q}{\rho} - \sqrt{p'(\rho)}, \quad \mu_2(\rho, q) = \frac{q}{\rho} + \sqrt{p'(\rho)},$$

where $q = \rho\, u$, and the eigenvectors are

$$r_1(\rho, q) = \begin{pmatrix} \rho \\ q - \rho\sqrt{p'(\rho)} \end{pmatrix}, \quad r_2(\rho, q) = \begin{pmatrix} \rho \\ q + \rho\sqrt{p'(\rho)} \end{pmatrix}.$$

The system is strictly hyperbolic in $\mathcal{D} = \{(\rho, q) : \rho > 0 \text{ or } q = 0\}$ with $\mu_1 < \mu_2$. It is genuinely nonlinear in both characteristic fields, i.e. $\nabla\mu_i \cdot r_i \neq 0$, i=1,2. The two functions $z_1 = z_1(\rho, q)$, $z_2 = z_2(\rho, q)$ are called the *Riemann invariants* of system (1) corresponding to μ_1 and μ_2 if they satisfy the equations

$$\nabla z_i \cdot r_i = 0, \quad i = 1, 2. \tag{23}$$

One solution of (23), when p follows the pressure law of isentropic gases (2) with $\gamma > 1$ is

$$z_1(\rho, q) = \frac{q}{\rho} + \alpha_\gamma\sqrt{p'(\rho)}, \quad z_2(\rho, q) = \frac{q}{\rho} - \alpha_\gamma\sqrt{p'(\rho)}, \quad \text{with } \alpha_\gamma = \frac{2}{\gamma - 1}. \tag{24}$$

For $\gamma = 1$, the Riemann invariants are given by

$$z_1(\rho, q) = \frac{q}{\rho} + \ln(\rho) \quad \text{and} \quad z_2(\rho, q) = \frac{q}{\rho} - \ln(\rho). \tag{25}$$

For clarity and generality, from now on we assume $\gamma > 1$, although all results also apply to the case $\gamma = 1$. While the expressions of the Riemann invariants differ in this latter case, the required assumptions are preserved.

Consider now the Riemann problem for (22), that is to say system (22) complemented with piecewise constant initial data such that

$$U(x, 0) = \begin{cases} U^- & \text{if} \quad x < 0, \\ U^+ & \text{if} \quad x > 0, \end{cases}$$

for two given constant left and right states $U^- = (\rho^-, q^-)$ and $U^+ = (\rho^+, q^+)$. The solution to the Riemann problem is then explicitly known and defined by an intermediate state $\hat{U} = (\hat{\rho}, \hat{q})$ verifying the following conditions:

i) The left state U^- is connected to $\hat{U}$ by a 1-shock or a 1-rarefaction wave such that

$$z_1(\rho^-, q^-) = z_1(\hat{\rho}, \hat{q}).$$

Moreover, shock waves satisfy $\mu_1(U^-) > \mu_1(\hat{U})$ (Lax admissibility condition) while rarefaction waves satisfy $\mu_1(U^-) < \mu_1(\hat{U})$. We then have a 1-shock if $\hat{\rho} > \rho^-$ and $z_1(\rho^-, q^-) = z_1(\hat{\rho}, \hat{q})$ or a 1-rarefaction if $\hat{\rho} < \rho^-$ and $z_1(\rho^-, q^-) = z_1(\hat{\rho}, \hat{q})$.

ii) The intermediate state $\hat{U}$ is connected to the right state U^+ by a 2-shock if $\hat{\rho} > \rho^+$ and $z_2(\hat{\rho}, \hat{q}) = z_2(\rho^+, q^+)$ or by a 2-rarefaction if $\hat{\rho} < \rho^+$ and $z_2(\hat{\rho}, \hat{q}) = z_2(\rho^+, q^+)$.

The intermediate state $\hat{U}$ is then uniquely defined if, in the (ρ, u)-plane, the following two curves $u_1(\rho) = u^- + \alpha_\gamma \left(\sqrt{p'(\rho^-)} - \sqrt{p'(\rho)}\right)$ and $u_2(\rho) = u^+ - \alpha_\gamma \left(\sqrt{p'(\rho^+)} - \sqrt{p'(\rho)}\right)$ intersect. Since $u_1(\rho)$ is strictly decreasing, unbounded, and starts at $u^- + \alpha_\gamma \sqrt{p'(\rho^-)}$ and $u_2(\rho)$ is strictly increasing, unbounded, with minimum $u^+ - \alpha_\gamma \sqrt{p'(\rho^+)}$, the Riemann problem has a unique solution in the region where

$$u^- + \alpha_\gamma \sqrt{p'(\rho^-)} \geq u^+ - \alpha_\gamma \sqrt{p'(\rho^+)}$$

or equivalently

$$z_1(\rho^-, q^-) \geq z_2(\rho^+, q^+). \tag{26}$$

Furthermore, we say that a state $(\rho, q) \in \mathcal{D} \backslash \{(0,0)\}$ is *subsonic* if $\mu_1(\rho, q) < 0 < \mu_2(\rho, q)$, *sonic* if $\mu_1(\rho, q) = 0$ or $\mu_2(\rho, q) = 0$ and *supersonic* if $\mu_1(\rho, q) < \mu_2(\rho, q) < 0$ or $0 < \mu_1(\rho, q) < \mu_2(\rho, q)$.

3.2. **The Riemann problem at the junction: the subsonic case.** Now, we shall consider a simple junction connecting two arcs as sketched in Figure 1. We use the same notation as in Section 2 and in particular, we shall use the subscript ℓ for the left arc and r for the right one.

Notations 3.1. *From now on, we shall use the following notations :*

- $U_\ell^- = (\rho_\ell^-, q_\ell^-)$ *and* $U_r^+ = (\rho_r^+, q_r^+)$ *denote the constant states on the left arc and on the right arc;*
- $U_\ell^* = (\rho_\ell^*, q_\ell^*)$ *and* $U_r^* = (\rho_r^*, q_r^*)$ *represent the unknown values of the left and right states at the junction.*

Following what has been done previously, we define the two sonic curves that determine the boundary between subsonic and supersonic regions, see the black curves on Figure 2, thanks to the following functions

$$\begin{cases} q_s^+(\rho) = \rho \sqrt{p'(\rho)}, \\ q_s^-(\rho) = -\rho \sqrt{p'(\rho)}. \end{cases} \tag{27}$$

We define the constant data $U_\ell^- = (\rho_\ell^-, q_\ell^-)$ and $U_r^+ = (\rho_r^+, q_r^+)$ given on the left and right arc respectively. We will assume that we are in the subsonic case at the junction, that is to say that $q_s^-(\rho_\ell^-) < q_\ell^- < q_s^+(\rho_\ell^-)$ and $q_s^-(\rho_r^+) < q_r^+ < q_s^+(\rho_r^+)$.

Now, in order to solve the Riemann problem, the unknown states U_ℓ^* and U_r^* at the junction have to lie on the Riemann invariant curves defined from U_ℓ^- and U_r^+. Considering the jump condition (JTC) in (3), and assuming that the states are all subsonic, we then get the following system of equations

$$\begin{cases} z_1(\rho_\ell^*, q_\ell^*) = z_1(\rho_\ell^-, q_\ell^-), \\ z_2(\rho_r^*, q_r^*) = z_2(\rho_r^+, q_r^+), \\ q_\ell^* = q_r^* = \kappa(\rho_\ell^* - \rho_r^*), \end{cases} \tag{28}$$

subject to the constraints

$$\begin{cases} q_s^-(\rho_\ell^*) < q_\ell^* < q_s^+(\rho_\ell^*), \\ q_s^-(\rho_r^*) < q_r^* < q_s^+(\rho_r^*). \end{cases} \tag{29}$$

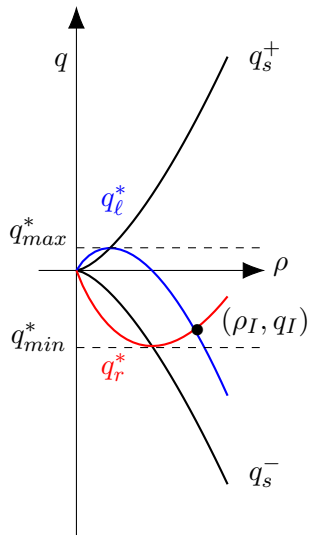

FIGURE 2. Riemann problem in the subsonic case with $p(\rho) = p_0\rho^2$ (i.e. $\gamma = 2$): sonic curves q_s^- and q_s^+ defined at Eq.(27) delimiting the subsonic region and Riemann invariant curves q_ℓ^* and q_r^* defined at Eq.(30)

Following Eq. (24), we define the Riemann invariant curves

$$\begin{cases} q_\ell^*(\rho) = z_1(\rho_\ell^-, q_\ell^-)\rho - \alpha_\gamma \rho\sqrt{p'(\rho)}, \\ q_r^*(\rho) = z_2(\rho_r^+, q_r^+)\rho + \alpha_\gamma \rho\sqrt{p'(\rho)}. \end{cases} \tag{30}$$

We notice that in the case where $1 < \gamma \leq 3$ and in the subsonic case, then $\mu_1(\rho_\ell^-, q_\ell^-) < 0 < \mu_2(\rho_r^+, q_r^+)$, implies $z_1(\rho_\ell^-, q_\ell^-) > 0 > z_2(\rho_r^+, q_r^+)$. Moreover, q_ℓ^* is a strictly concave function of ρ and q_r^* is strictly convex. Thus condition (26) holds and there exists a unique intersection point, apart from 0, for the two curves of functions q_ℓ^* and q_r^*. From now on, we shall call this point $U_I = (\rho_I, q_I)$ and it satisfies $q_I = q_\ell^*(\rho_I) = q_r^*(\rho_I)$.

Now, in the case of the conditions (28) we consider here, we may allow a discontinuity on densities, i.e. $\rho_\ell^* \neq \rho_r^*$. In the next lemma, we shall show that system (28), subject to (29), admits a unique solution, which lies therefore in the *subsonic* region.

Lemma 3.1. *We assume p of the form (2) with $1 \leq \gamma \leq 3$. Let be given two points $U_\ell^- = (\rho_\ell^-, q_\ell^-)$ and $U_r^+ = (\rho_r^+, q_r^+)$ such that $q_s^-(\rho_\ell^-) < q_\ell^- < q_s^+(\rho_\ell^-)$ and $q_s^-(\rho_r^+) < q_r^+ < q_s^+(\rho_r^+)$, then there exists a unique couple of points U_ℓ^*, U_r^* verifying system (28) subject to constraints (29).*

Proof. First of all, we assume $\gamma > 1$ and note that the solution $q^* = q_\ell^*(\rho_\ell^*) = q_r^*(\rho_r^*)$ to system (28) should be sought, see Figure2, in the region defined by

$$\{q : q_{min}^* = \min_{\rho>0} q_r^*(\rho) \leq q \leq \max_{\rho>0} q_\ell^*(\rho) = q_{max}^*\}.$$

Note that the intersection point (ρ_I, q_I) satisfies $q_{min}^* < q_I < q_{max}^*$.

Then, it is easy to check that the intersection point, apart from 0, between the sonic curve defined by q_s^+ and the curve defined by q_ℓ^* coincides with the maximum point for q_ℓ^*. Indeed,

$$q_s^+(\rho) = q_\ell^*(\rho) \text{ and } \rho > 0 \quad \Longleftrightarrow \quad \sqrt{p'(\rho)} = \frac{\gamma-1}{\gamma+1}\, z_1(\rho_\ell^-, q_\ell^-)$$

and

$$(q_\ell^*)'(\rho) = 0 \quad \Longleftrightarrow \quad \sqrt{p'(\rho)} = \frac{\gamma-1}{\gamma+1}\, z_1(\rho_\ell^-, q_\ell^-).$$

Analogously, the minimum point for q_r^* coincides with the intersection point, apart from 0, between the sonic curve defined by q_s^- and the curve defined by q_r^*.

Therefore, in the subsonic region, q_ℓ^* (resp. q_r^*) is a continuous and strictly decreasing (resp. strictly increasing) function of ρ and we can therefore define its inverse function ϕ_ℓ (resp. ϕ_r), which is also a continuous and strictly decreasing (resp. strictly increasing) function of q.

We can now prove that for all $\kappa \in [0, +\infty)$ there exists a unique solution to system (28) subject to subsonic conditions (29).

Such a solution satisfies $\rho_\ell^* = \phi_\ell(q^*)$, $\rho_r^* = \phi_r(q^*)$ and $q^* = \kappa(\rho_\ell^* - \rho_r^*) = \kappa\big(\phi_\ell(q^*) - \phi_r(q^*)\big)$ and the existence and unicity of the solution follows from the fact that the function K defined by

$$K(q) = \frac{q}{\phi_\ell(q) - \phi_r(q)}$$

is continuous and strictly monotone, i.e. we have that

(i) if $q_I > 0$ then $K : [0, q_I] \to [0, +\infty)$ is continuous and strictly increasing;
(ii) if $q_I < 0$ then $K : [q_I, 0] \to [0, +\infty)$ is continuous and strictly decreasing.

The proof also holds in the isothermal case, when $\gamma = 1$ and the Riemann invariants are given by (25). Specifically, the functions $q_\ell^* = -\rho \ln \rho + \rho z_1^-$ and $q_r^* = \rho \ln \rho + \rho z_2^+$ satisfy the required assumptions. Indeed, they are strictly concave and strictly convex, respectively. Their extrema coincide with the intersection of the corresponding invariant with the sonic curve (which, in this case, is $q = \rho$). Consequently, q_ℓ^* is strictly decreasing and invertible in the subsonic region, whereas q_r^* is strictly increasing and invertible in the subsonic region. □

Staying in the subsonic region is equivalent to limiting the amplitude of the jump, specifically for $\kappa \to 0$ then $q^* \to 0$ which belongs to the subsonic region and for $\kappa \to +\infty$ then $q^* \to q_I$ and the jump amplitude goes to zero, i.e. $\rho_\ell^* - \rho_r^* \to 0$.

Remark 3.1. *When $\gamma > 3$, if we impose condition* (26) *for the left and right states, the intersection point q_I exists and system* (28) *admits a solution, but we cannot guarantee that this solution is subsonic.*

3.3. **Riemann invariants and the junction - the supersonic case.** In the supersonic case, the Riemann solver leading to system (28) does not apply. A different formulation is needed, which in general is still an open problem. A number of possible approaches have been proposed in the literature, see for instance [45], but here we follow the approach proposed in [17]. The idea stated in this paper can be resumed as follows :

- Assume to be on a left arc and to have to the left of the junction a supersonic state U_ℓ^- with $\mu_1(\rho_\ell^-, q_\ell^-) > 0$, namely $q_\ell^- > q_s^+(\rho_\ell^-)$. Introducing the point $\widetilde{U}_\ell^- = (\widetilde{\rho}_\ell^-, \widetilde{q}_\ell^-)$ such that $\widetilde{q}_\ell^- = q_\ell^-$, $z_1(\widetilde{\rho}_\ell^-, q_\ell^-) = z_1(\rho_\ell^-, q_\ell^-)$ and $\mu_1(\widetilde{U}_\ell^-) < 0$, the region of possible junction

values U_ℓ^* is defined as the set of points verifying

$$z_1(\rho_\ell^*, q_\ell^*) = z_1(\widetilde{\rho}_\ell^-, q_\ell^-) \quad \text{with} \quad \rho_\ell^* > \widetilde{\rho}_\ell^- .$$

- Assume to be on a right arc and to have to the right of the junction a supersonic state U_r^+ with $\mu_2(\rho_r^+, q_r^+) < 0$, namely $q_r^+ < q_s^-(\rho_r^+)$. Introducing the point $\widetilde{U}_r^+ = (\widetilde{\rho}_r^+, \widetilde{q}_r^+)$ such that $\widetilde{q}_r^+ = q_r^+$, $z_2(\widetilde{\rho}_r^+, q_r^+) = z_2(\rho_r^+, q_r^+)$ and $\mu_2(\widetilde{U}_r^+) > 0$, the region of possible junction values U_r^* is defined as the set of points verifying

$$z_2(\rho_r^*, q_r^*) = z_2(\widetilde{\rho}_r^+, q_r^+) \quad \text{with} \quad \rho_r^* < \widetilde{\rho}_r^+ .$$

To summarize, on the one hand, if we are in the supersonic region with $\mu_1(\rho_\ell^-, q_\ell^-) > 0$ (resp. $\mu_2(\rho_r^+, q_r^+) < 0$) the idea is to connect first the left (resp. right) state U_ℓ^- (resp. U_r^+) with a shock with zero speed to the subsonic state $\widetilde{U}_\ell^-$ (resp. $\widetilde{U}_r^+$), i.e. $\dfrac{q_\ell^- - \widetilde{q}_\ell^-}{\rho_\ell^- - \widetilde{\rho}_\ell^-} = 0$ (resp. $\dfrac{q_r^+ - \widetilde{q}_r^+}{\rho_r^+ - \widetilde{\rho}_r^+} = 0$), and then the latter to U_ℓ^* (resp. U_r^*) with a shock with negative (resp. positive) speed.

On the other hand, if we are in the supersonic region with $\mu_1(\rho_\ell^-, q_\ell^-) < 0$, that is q_ℓ^- is negative and $q_\ell^- < q_s^-(\rho_\ell^-)$ (resp. $\mu_2(\rho_r^+, q_r^+) > 0$, namely q_r^+ is positive and $q_r^+ > q_s^+(\rho_r^+)$), see Figure 3, an admissible solution in the sense of the definition of Riemann solver given in [17] is to stay on the invariant curve $z_1(\rho_\ell^*, q_\ell^*) = z_1(\rho_\ell^-, q_\ell^-)$ (resp. $z_2(\rho_r^*, q_r^*) = z_2(\rho_r^+, q_r^+)$) with the constraint $\mu_2(\rho_\ell^*, q_\ell^*) < 0$ (resp. $\mu_1(\rho_r^*, q_r^*) > 0$).

Moreover, in both cases, the values U_ℓ^* and U_r^* have to verify the jump condition (3). It is clear that this procedure does not always lead to a solution. However, as stated in [17], the region of admissible junction solutions may be enlarged but losing the uniqueness, and additional conditions have to be added to define the solution at a junction. This discussion is beyond the scope of our work, and we will simply compare simulations in cases where the above procedure is well defined.

Remark 3.2. *Numerical examples of Riemann solutions are displayed in section 5:*

- *in Test C1, we consider a subsonic initial datum, both on left and right arcs, see results at Fig.5;*
- *in Test C3, we consider an initial datum, which is subsonic on the left arc and supersonic on the right arc, see results at Fig.7.*

4. A relaxation scheme for the jump junction condition - case of a 2-arc network

For the sake of simplicity, we explain in this section the numerical scheme and the numerical jump junction condition we develop in the case of a simple network, composed of two arcs. An extension to more general networks will be detailed in Section 6.

4.1. **A relaxation scheme on a single interval.**

Now, let us describe the numerical scheme we use to approximate (11)–(3). To begin with, we use a relaxation scheme, first introduced in [46], see also [3, 52, 4, 10], which we will see, away from the junction, is just another interpretation of the HLL scheme introduced in [42].

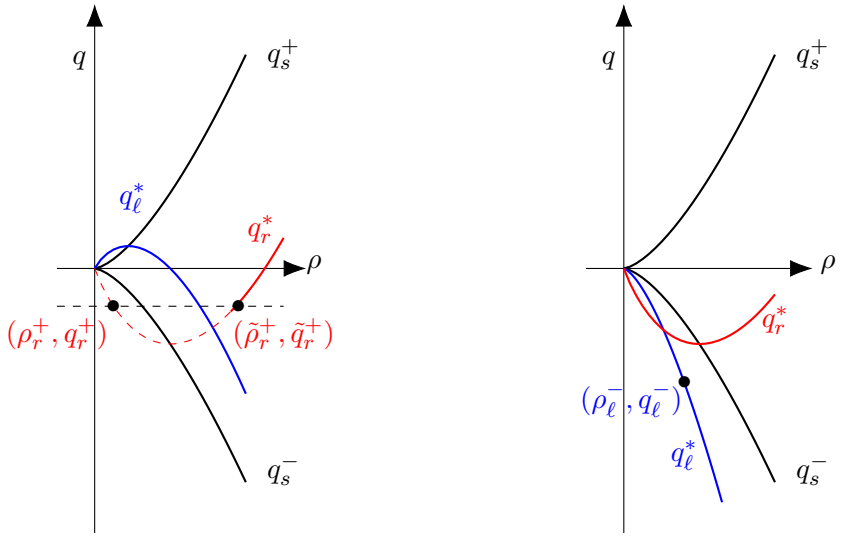

FIGURE 3. Riemann problem in the supersonic case with $p(\rho) = p_0\rho^2$: on the left, right supersonic case with $\mu_2(\rho_r^+, q_r^+) < 0$, i.e. $q_r^+ < q_s^-(\rho_r^+)$, and construction of the point $\widetilde{U}_r^+ = (\widetilde{\rho}_r^+, \widetilde{q}_r^+)$. On the right, left supersonic case with $\mu_1(\rho_\ell^-, q_\ell^-) < 0$, i.e. $q_\ell^- < q_s^-(\rho_\ell^-)$; here, we stay on the invariant curve q_ℓ^*.

We rewrite our equations in the vector form already presented in Section 3, the same as equation (22):

$$\partial_t U + \partial_x F(U) = 0, \tag{31}$$

where $U \in \mathbb{R}^2$ is the vector of unknowns, and the function $F : \mathbb{R}^2 \to \mathbb{R}^2$ is the flux of the system.

Now, we introduce its relaxation approximation, namely a semilinear hyperbolic system with a singular perturbation parameter ϵ:

$$\begin{cases} \partial_t f_1^\epsilon + c_1 \partial_x f_1^\epsilon = \dfrac{1}{\epsilon}\left(M_1(U^\epsilon) - f_1^\epsilon\right), \\ \\ \partial_t f_2^\epsilon + c_2 \partial_x f_2^\epsilon = \dfrac{1}{\epsilon}\left(M_2(U^\epsilon) - f_2^\epsilon\right). \end{cases} \tag{32}$$

Here $c_1,\ c_2$ are real constants such that $c_1 < c_2$, $f_i^\epsilon \in \mathbb{R}^2$, for $i = 1, 2$, and $U^\epsilon := f_1^\epsilon + f_2^\epsilon$. The functions $M_i(U) : \mathbb{R}^2 \to \mathbb{R}^2$, for $i = 1, 2$, are called Maxwellians for the system and are vector functions satisfying the two following relations :

$$\begin{cases} M_1(U) + M_2(U) & = U, \\ \\ c_1 M_1(U) + c_2 M_2(U) & = F(U). \end{cases} \tag{33}$$

From (33), we can obtain explicit expressions for $M_1(U)$ and $M_2(U)$ as

$$M_1(U) = \frac{c_2 U - F(U)}{c_2 - c_1} \quad \text{and} \quad M_2(U) = \frac{c_1 U - F(U)}{c_1 - c_2}. \tag{34}$$

Notice that, setting $V^\epsilon = c_1 f_1^\epsilon + c_2 f_2^\epsilon$, from system (32) we easily obtain

$$\begin{cases} \partial_t U^\epsilon + \partial_x V^\epsilon = 0, \\ \\ \partial_t V^\epsilon + \partial_x \left((c_1 + c_2) V^\epsilon - c_1 c_2 U^\epsilon \right) = \dfrac{1}{\epsilon} \left(F(U^\epsilon) - V^\epsilon \right). \end{cases}$$

So, as ϵ goes to zero, we expect U^ϵ converges to the solution to (31), as shown for the scalar case in [52], see also [58, 9, 8] for the system case in one space dimension. Clearly, when $c_1 = -\lambda < 0 < c_2 = \lambda$, for some real constant $\lambda > 0$, we recover the classical Jin-Xin model of relaxation [46].

Notice that, as shown in [9] (see also [4]), a necessary condition to have the stability for this approximation is that the Jacobians of the Maxwellian functions $M_i(U)$, are strictly positive matrices for $i = 1, 2$ and all values of U under consideration. Using the explicit expression (34), it is easy to see that the so-called subcharacteristic condition has to be verified. Namely, if $\mu(U)$ is a real eigenvalue of the Jacobian matrix $F'(U)$, we need to have that

$$c_1 \leq \mu(U) \leq c_2 \text{ for all } U \text{ under consideration.} \tag{35}$$

This condition will be required not only to assess the consistency of the correspondent scheme, but also its stability.

The strategy to use this relaxation approach to create a numerical scheme for equation (31), is in general to solve numerically at each time step the homogeneous part of system (32)

$$\begin{cases} \partial_t f_1 + c_1 \partial_x f_1 = 0, \\ \\ \partial_t f_2 + c_2 \partial_x f_2 = 0, \end{cases}$$

and then to reconstruct the solution to (31) from a suitable projection of the functions (f_1, f_2) on the Maxwellian functions $M_1(U), M_2(U)$. This strategy has been fully implemented in [4] in the framework of Finite Difference schemes, see also the recent developments in the framework of Lattice Boltzmann schemes in [2]. In the following, as already done in [53], we prefer to follow the Finite Volume approach of [10]. So, let us introduce some notations to present our scheme.

We begin by describing the discretization process on a single interval, which will be the numerical strategy that we will use both on arc ℓ and on arc r.

Let us denote by Δx the spatial discretization step. We discretize the interval using J cells

$$\mathcal{C}_j = [x_{j-1/2}, x_{j+1/2}],\ 1 \leq j \leq J$$

centered at the nodes $x_j = (j - \frac{1}{2})\Delta x$, $1 \leq j \leq J$.

We also denote by Δt the time step. Discrete times are denoted by $t_n = n\Delta t, n \in \mathbb{N}$. The time index will be omitted when possible for the sake of simplicity.

Consider system (1) under the form (31). We define U_j^n to be the approximation of the mean value of vector U on cell $\mathcal{C}_j$ at time t_n, that is to say $U_j^n \sim \dfrac{1}{\Delta x} \displaystyle\int_{\mathcal{C}_j} U(t^n, x) dx$. According to the finite volume framework, an explicit conservative finite volume scheme for discretizing equation (31) can be expressed as follows

$$U_j^{n+1} = U_j^n - \frac{\Delta t}{\Delta x} \left(\mathcal{F}_{j+1/2}^n - \mathcal{F}_{j-1/2}^n \right), \tag{36}$$

with $\mathcal{F}^n_{j+1/2} = \mathcal{F}(U^n_j, U^n_{j+1})$ for an explicit three point scheme. The scheme is therefore defined by the function $\mathcal{F}$ such that $\mathcal{F}(U^-, U^+) = \begin{pmatrix} \mathcal{F}^\rho(U^-, U^+) \\ \mathcal{F}^q(U^-, U^+) \end{pmatrix} \in \mathbb{R}^2$, which is called the *numerical flux*.

We now describe the scheme we will use on each arc, which will be equivalent to the HLL scheme. Here we follow the presentation given in [10].

Consider again the homogeneous counterpart to the *relaxation system* (32), with $f_i = f_i(x,t) \in \mathbb{R}^2$ for $i = 1, 2$,

$$\begin{cases} \partial_t f_1 + c_1 \partial_x f_1 = 0, \\ \\ \partial_t f_2 + c_2 \partial_x f_2 = 0, \end{cases} \tag{37}$$

where $c_1 < c_2$ are two speeds to be chosen later on.

Noticing that system (37) can be solved explicitly, we obtain an approximate solution to system (31) as a function of the solution to system (37). Indeed, an exact Riemann solver for (37) gives

$$\mathcal{R}(x/t, f^-, f^+) = \begin{cases} (f_1^-, f_2^-) & \text{if} \quad x/t < c_1, \\ (f_1^+, f_2^-) & \text{if} \quad c_1 < x/t < c_2, \\ (f_1^+, f_2^+) & \text{if} \quad c_2 < x/t, \end{cases} \tag{38}$$

with $f_i^\pm \sim M_i(U^\pm)$, $i = 1, 2$. Thus we get the following approximate HLL numerical flux for the scheme in conservative form (36)

(39)

$$\mathcal{F}(U^-, U^+) = \begin{cases} c_1 M_1(U^-) + c_2 M_2(U^-) = F(U^-), & \text{if } 0 < c_1, \\ c_1 M_1(U^+) + c_2 M_2(U^-) = \dfrac{c_2 F(U^-) - c_1 F(U^+)}{c_2 - c_1} + \dfrac{c_2 c_1}{c_2 - c_1}(U^+ - U^-) & \\ \qquad\qquad\qquad\qquad\qquad\qquad\qquad\qquad\qquad\qquad \text{if } c_1 < 0 < c_2, & \\ c_1 M_1(U^+) + c_2 M_2(U^+) = F(U^+), & \text{if } c_2 < 0. \end{cases}$$

Note that for stability reasons and to have some entropy dissipation, c_1 and c_2 have to be chosen accordingly to the inequality (35).

From now on, to deal with the transmission condition (JTC), we always stay in the case $c_1 < 0 < c_2$. For simplicity reasons, we set $c_2 = -c_1 = \lambda$ with $\lambda > \max_U |\mu(U)| > 0$, where $\mu(U)$ is the maximal eigenvalue of $F'(U)$, even if the same considerations could be made in the general case. The numerical flux (39) therefore reduces to

$$\mathcal{F}(U^-, U^+) = \frac{F(U^-) + F(U^+)}{2} - \frac{\lambda}{2}(U^+ - U^-) \tag{40}$$

and the Maxwellian functions (34) to

$$M_1(U) = \frac{1}{2}\left(U - \frac{F(U)}{\lambda}\right) \quad \text{and} \quad M_2(U) = \frac{1}{2}\left(U + \frac{F(U)}{\lambda}\right). \tag{41}$$

Finally, let us describe the discrete numerical boundary conditions in the case of a single interval. We assume that system (31) is complemented with Neumann boundary conditions on both extremities, which guarantee the mass conservation, that is to say $\partial_x \rho(t, 0) = q(t, 0) = 0$ and $\partial_x \rho(t, L) = q(t, L) = 0$ for all $t \geq 0$.

In the discrete setting, we have to define the quantities in the external ghost cells of the network, $\mathcal{C}_0$ and $\mathcal{C}_{J+1}$. To ensure the mass conservation also at the discrete level, we impose on both boundaries

$$\begin{cases} \mathcal{F}^\rho(U_0, U_1) = \dfrac{1}{2}(q_0 + q_1) - \dfrac{\lambda}{2}(\rho_1 - \rho_0) = 0, \\ \mathcal{F}^\rho(U_J, U_{J+1}) = \dfrac{1}{2}(q_J + q_{J+1}) - \dfrac{\lambda}{2}(\rho_{J+1} - \rho_J) = 0, \end{cases}$$

see Eq. (40), which is satisfied if

$$\rho_0 = \rho_1 \text{ and } q_0 = -q_1 \tag{42}$$

and

$$\rho_J = \rho_{J+1} \text{ and } q_J = -q_{J+1}. \tag{43}$$

4.2. **The relaxation scheme on a 2-arc network.** Let us now go back to the case of a simple network with two arcs sketched in Figure 1.

We still denote by Δx the spatial discretization step, that we assume to be the same for both arcs for simplicity reasons and by Δt the time step. We discretize the left arc (resp. right arc) using J_ℓ (resp. J_r) cells

$$\mathcal{C}_{j,\ell} = [x_{j-1/2,\ell}, x_{j+1/2,\ell}],\ 1 \le j \le J_\ell \quad (\text{resp. } \mathcal{C}_{j,r} = [x_{j-1/2,r}, x_{j+1/2,r}],\ 1 \le j \le J_r)$$

centered at the nodes $x_{j,\ell} = (j - \frac{1}{2})\Delta x$, $1 \le j \le J_\ell$ (resp. $x_{j,r} = (j - \frac{1}{2})\Delta x$, $1 \le j \le J_r$).

On each arc we solve the system (31) by the approximation (36)-(40) with $\lambda = \lambda_\ell$ and $\lambda = \lambda_r$ for arc ℓ and arc r respectively. Again, more general speeds could be considered, but we limit this presentation to the simplest case.

Boundary conditions at the extremities of the network are simply deduced from (42)-(43), that is to say

$$\rho_{0,\ell} = \rho_{1,\ell} \text{ and } q_{0,\ell} = -q_{1,\ell}. \tag{44}$$

and

$$\rho_{J_r,r} = \rho_{J_r+1,r} \text{ and } q_{J_r,r} = -q_{J_r+1,r}. \tag{45}$$

4.3. **Numerical treatment of the junction.** The current objective is to establish precise and consistent conditions at the junction of the two arcs, that is to say *consistent* values for the ghost cells at the junction, $\mathcal{C}_{J_\ell+1,\ell}$ and $\mathcal{C}_{0,r}$.

Notations 4.1. *From now on we shall use the following notations, see notations in blue in Figure 4 :*

- $U_\ell^* = (\rho_\ell^*, q_\ell^*)$ *and* $U_r^* = (\rho_r^*, q_r^*)$ *represent the unknown values at the junction on the ghost cell* $\mathcal{C}_{J_\ell+1,\ell}$ *on arc* ℓ *and on the cell* $\mathcal{C}_{0,r}$ *on arc* r*, respectively;*
- $U_\ell^- = (\rho_\ell^-, q_\ell^-) = (\rho_{J_\ell,\ell}, q_{J_\ell,\ell})$ *denotes the values on the last cell* $\mathcal{C}_{J_\ell,\ell}$ *on arc* ℓ*;*
- $U_r^+ = (\rho_r^+, q_r^+) = (\rho_{1,r}, q_{1,r})$ *stands for values on the first cell* $\mathcal{C}_{1,r}$ *on arc* r*,*
- *the notation* $v_{j,a}^n$ *will be employed to denote variable* v *(*$v = \rho$ *or* q*) with* j *the cell index,* a *denotes the arc and can take the values* $a = \ell$ *or* $a = r$ *and* n *denotes the time index;*
- *in the relaxation setting,* $f_{i,\ell}^-$ *and* $f_{i,r}^+$*,* $i = 1, 2$*, denote the left and right states and* $f_{i,\ell}^*$ *and* $f_{i,r}^*$*,* $i = 1, 2$*, denote the left and right intermediate states, see Figure 4.*

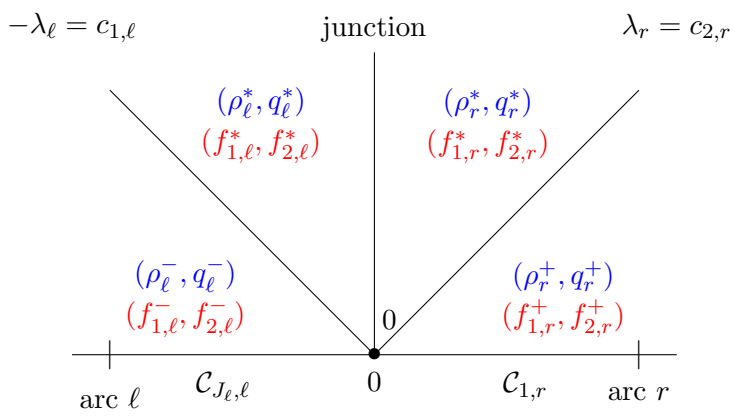

FIGURE 4. Notations for the quantities at the junction : in blue, (ρ_ℓ^-, q_ℓ^-) and (ρ_r^+, q_r^+) are the left and right states and (ρ_ℓ^*, q_ℓ^*) and (ρ_r^*, q_r^*) the two intermediate states. In red, the two corresponding vectors f_1 and f_2 for the relaxation approximation.

Therefore, to complement the scheme described in Section 4.2, we need now to find some values for the four quantities at the junction, i.e. $q_\ell^*, q_r^*, \rho_\ell^*$ and ρ_r^*. As stated above, we need to impose some transmission conditions at the junction. We consider a discrete version of the equality of the fluxes (15) in order to have the mass conservation at the junction and the (JTC) transmission conditions (3) linking the fluxes with the difference of densities. Namely, with the notations introduced above,

$$q_\ell^* = q_r^* = \kappa(\rho_\ell^* - \rho_r^*).$$

Since we have a total of 4 unknowns to be found at the junction, we need to impose two supplementary conditions. Let us now consider the relaxation system (37) on both arcs ℓ and r with $c_{1,\ell} = -c_{2,\ell} = \lambda_\ell > 0$ and $c_{1,r} = -c_{2,r} = \lambda_r > 0$ respectively. By the exact Riemann solver (38) at the junction, we get

$$f_{2,\ell}^* = f_{2,\ell}^- \text{ on arc } \ell, \tag{46}$$

$$f_{1,r}^* = f_{1,r}^+ \text{ on arc } r, \tag{47}$$

where here $f_{i,\ell}^*$ (resp. $f_{i,r}^*$), $i = 1, 2$ represents the (unknown) value of the solution for $-\lambda_l < x/t < 0$ (resp. for $0 < x/t < \lambda_r$), $f_{i,\ell}^-$ is the solution for $x/t < -\lambda_\ell$ on arc ℓ and $f_{i,r}^+$ the solution for $x/t > \lambda_r$ on arc r.

Switching to the first components of maxwellian functions given by (41), we can rewrite (46) and (47) as

$$\begin{cases} \dfrac{1}{2}\left(\rho_\ell^* + \dfrac{q_\ell^*}{\lambda_\ell}\right) = \dfrac{1}{2}\left(\rho_\ell^- + \dfrac{q_\ell^-}{\lambda_\ell}\right), \\ \dfrac{1}{2}\left(\rho_r^* - \dfrac{q_r^*}{\lambda_r}\right) = \dfrac{1}{2}\left(\rho_r^+ - \dfrac{q_r^+}{\lambda_r}\right), \end{cases}$$

which gives us the two extra conditions at the junction we were looking for.

In summary, at the junction, we need to solve the following linear system for the unknowns $q^* = q_\ell^* = q_r^*,\ \rho_\ell^*$ and ρ_r^* :

$$\left\{\begin{array}{l} q^* = \kappa(\rho_\ell^* - \rho_r^*), \\ \rho_\ell^* + \dfrac{q^*}{\lambda_\ell} = \rho_\ell^- + \dfrac{q_\ell^-}{\lambda_\ell}, \\ \rho_r^* - \dfrac{q^*}{\lambda_r} = \rho_r^+ - \dfrac{q_r^+}{\lambda_r}. \end{array}\right. \tag{48}$$

This system can be solved explicitely as :

$$\left\{\begin{array}{l} q^* = q_\ell^* = q_r^* = \frac{\kappa}{\kappa(\lambda_\ell+\lambda_r)+\lambda_\ell\lambda_r}(\lambda_r q_\ell^- + \lambda_\ell q_r^+ + \lambda_\ell\lambda_r(\rho_\ell^- - \ \rho_r^+)), \\ \rho_r^* = \rho_r^+ + \frac{1}{\lambda_r}(q^* - q_r^+), \\ \rho_\ell^* = \rho_\ell^- - \frac{1}{\lambda_\ell}(q^* - q_\ell^-). \end{array}\right. \tag{49}$$

The solution can then be used as boundary values for the arcs on the ghost cells at the junction.

Notice that, the system given by (48) describing the quantities at the junction, can be recovered looking at the numerical flux $\mathcal{F}$ by considering directly the discretization of system (11)-(3).

We still use here the previous notations, namely, we denote by $U_\ell^- = (\rho_\ell^-, q_\ell^-) = (\rho_{J_\ell,\ell}, q_{J_\ell,\ell})$ (resp. $U_r^+ = (\rho_r^+, q_r^+) = (\rho_{1,r}, q_{1,r})$) the values on the last cell $\mathcal{C}_{J_\ell,\ell}$ on arc ℓ (resp. on the first cell $\mathcal{C}_{1,r}$ on arc r).

At the junction, the mass conservation at the discrete level gives the condition

$$\mathcal{F}^\rho(U_\ell^-, U_\ell^*) = \mathcal{F}^\rho(U_r^*, U_r^+) \tag{50}$$

that is coupled with the following relations, coming from the discretization of conditions (3) :

$$\mathcal{F}^\rho(U_\ell^-, U_\ell^*) = \mathcal{F}^\rho(U_r^*, U_r^+) = \kappa(\rho_\ell^* - \rho_r^*).$$

Again, we have 4 unknowns at the junction and we need two supplementary conditions. We find them by imposing the equality between the numerical flux for the mass equation $F^\rho = \rho u = q$ and the numerical discretization for the momentum $q = \rho u$, namely :

$$\mathcal{F}^\rho(U_\ell^-, U_\ell^*) = q_\ell^*, \quad \mathcal{F}^\rho(U_r^*, U_r^+) = q_r^*. \tag{51}$$

We obtain therefore a linear system of 4 equations with 4 unknowns :

$$\left\{\begin{array}{l} \mathcal{F}^\rho(U_\ell^-, U_\ell^*) = \mathcal{F}^\rho(U_r^*, U_r^+) = \kappa(\rho_\ell^* - \rho_r^*), \\ \mathcal{F}^\rho(U_\ell^-, U_\ell^*) = q_\ell^*, \\ \mathcal{F}^\rho(U_r^*, U_r^+) = q_r^*. \end{array}\right. \tag{52}$$

Note that system (52) holds for any numerical flux $\mathcal{F}$ and not only for the HLL flux.

Remark 4.1. *In the case of the HLL numerical flux, the previous system* (52) *becomes*

$$\left\{\begin{array}{l} q^* = q_\ell^* = q_r^* = \kappa(\rho_\ell^* - \rho_r^*), \\ \dfrac{q_\ell^- + q^*}{2} - \dfrac{\lambda_\ell}{2}(\rho_\ell^* - \rho_\ell^-) = q^*, \\ \dfrac{q^* + q_r^+}{2} - \dfrac{\lambda_r}{2}(\rho_r^+ - \rho_r^*) = q^*, \end{array}\right. \tag{53}$$

which is the same as system (48)*. In this setting, the two formulations are equivalent.*

Remark 4.2. *Let us briefly compare the two junction conditions that have been considered in this paper, i.e. system* (48) *and system* (28)*.*

- *Note that system* (48) *admits always a solution, both for subsonic and supersonic states, unlike system* (28)*. It can therefore be seen as an extension of system* (28) *that works in both cases.*
- *Then, Riemann conditions leading to system* (28) *should not preserve the mass conservation at the discrete level, although conditions in system* (48) *are designed to do so.*
- *Finally, the reasoning for Riemann conditions at Subsection 3.2 only holds for a power* γ *in Eq.*(2) *such that* $1 < \gamma \leq 3$*, whereas system* (48) *holds a solution for every* $\gamma > 1$*. Note that the parameter* γ *is only present in Eq.*(48) *through the values of* λ_ℓ *and* λ_r*.*

Remark 4.3. *In the subsonic region, the two last conditions given in* (48) *may be viewed as a local linearization of relations* (30)*. In fact, substituting* (30) *with the tangent lines of the two Riemann invariants in the points* (ρ_ℓ^-, q_ℓ^-) *and* (ρ_r^+, q_r^+) *respectively, we get*

$$\begin{cases} q_\ell^*(\rho) = q_\ell^- + \mu_1(\rho_\ell^-, q_\ell^-)(\rho - \rho_\ell^-), \\ q_r^*(\rho) = q_r^+ + \mu_2(\rho_r^+, q_r^+)(\rho - \rho_r^+). \end{cases} \tag{54}$$

On the other hand, the two last equations in (48) *can be rewritten as*

$$\begin{cases} q_\ell^* = q_\ell^- - \lambda_\ell(\rho_\ell^* - \rho_\ell^-), \\ q_r^* = q_r^+ + \lambda_r(\rho_r^* - \rho_r^+). \end{cases} \tag{55}$$

Then, the two unknown values U_ℓ^* *and* U_r^* *belong to the decreasing line* $q(\rho) = q_\ell^- - \lambda_\ell(\rho - \rho_\ell^-)$ *and to the increasing line* $q(\rho) = q_r^+ + \lambda_r(\rho - \rho_r^+)$ *respectively. Since we are assuming* $\mu_1(\rho_\ell^-, q_\ell^-) < 0$ *and* $\mu_2(\rho_r^+, q_r^+) > 0$*,* (54) *reads as*

$$\begin{cases} q_\ell^* = q_\ell^- - |\mu_1(\rho_\ell^-, q_\ell^-)|(\rho_\ell^* - \rho_\ell^-), \\ q_r^* = q_r^+ + \mu_2(\rho_r^+, q_r^+)(\rho_r^* - \rho_r^+). \end{cases} \tag{56}$$

The two systems (55) *and* (56) *differ only in the choice of the angular coefficient of the two lines.*

4.4. **Consistency properties of the numerical scheme.**

4.4.1. *Mass conservation.* First we prove the following property, which is equivalent to the continuous mass preservation (14).

Proposition 4.1. *Let us consider system* (11)–(3) *set on a* 2*-arc network displayed in Figure1 with boundary conditions* (13) *on the outer nodes and junction conditions* (3)*. The numerical scheme* (36) *with discrete boundary conditions* (44)-(45) *on the outer nodes and discrete junction conditions* (52) *is mass-preserving, that is to say the discrete mass* $m^n = h\sum_{j=1}^{J_\ell} \rho_{j,\ell}^n + h\sum_{j=1}^{J_r} \rho_{j,r}^n$ *is independent of* $n \in \mathbb{N}$*.*

Proof. We consider the first component of equation (36). The conservation of the discrete mass is given by the boundary conditions for the outer nodes (44)-(45) and by condition (50) at the junction. □

4.4.2. *Positivity of the solution.* Now, we prove that the positivity of the solution is preserved in the particular case of HLL numerical flux :

Proposition 4.2. *Let us consider scheme* (36) *with flux* (40)*, boundary conditions* (44) – (45) *and condition* (53) *at the junction in order to discretize system* (11)-(3) *on a* 2*-arc network. We define* $\lambda_\ell^n > 0$ *(resp.* $\lambda_r^n > 0$*) such that*

$$\lambda_\ell^n \geq \max_{1\leq j\leq J_\ell} |u_{j,\ell}^n| + \sqrt{p'(\rho_{j,\ell}^n)}(\ \textit{resp.}\ \lambda_r^n \geq \max_{1\leq j\leq J_r} |u_{j,r}^n| + \sqrt{p'(\rho_{j,r}^n)}). \tag{57}$$

If the initial condition is positive, that is to say

$$\rho_{j,\ell}^0 \geq 0 \textit{ for all } 1\leq j\leq J_\ell\ (\ \textit{resp.}\ \rho_{j,r}^0 \geq 0 \textit{ for all } 1\leq j\leq J_r),$$

then the solution remains positive in time, that is to say

$$\rho_{j,\ell}^n \geq 0 \textit{ for all } 1\leq j\leq J_\ell\ (\ \textit{resp.}\ \rho_{j,r}^n \geq 0 \textit{ for all } 1\leq j\leq J_r),\ \textit{for all } n\in\mathbb{N}.$$

Notice that condition (57) is just a formulation in this case of condition (35), which is necessary to obtain the stability of the numerical scheme.

Proof. We prove the proposition by induction.

Assume that $\rho_{j,\ell}^n \geq 0$ for all $1\leq j\leq J_\ell$ (resp. $\rho_{j,r}^n \geq 0$ for all $1\leq j\leq J_r$). Since $\lambda_\ell^n \geq |u_{j,\ell}^n|$ for all $1\leq j\leq J_\ell$ (resp. $\lambda_r^n \geq |u_{j,r}^n|$ for all $1\leq j\leq J_r$), we use the explicit expressions obtained at Eq.(49) to prove that $\rho_r^{*,n} \geq 0$ and $\rho_\ell^{*,n} \geq 0$. From these two inequalities, we demonstrate that $\rho_{j,\ell}^{n+1} \geq 0$ for all $1\leq j\leq J_\ell$ (resp. $\rho_{j,r}^{n+1} \geq 0$ for all $1\leq j\leq J_r$). □

5. Numerical tests in the case of a 2-arc network

In this section, we examine the characteristics of the numerical method proposed in Section 4 and we evaluate its accuracy by examining a simple network consisting of two arcs. The pressure is given by the pressure law given at Eq.(2) with $\gamma = 2$, unless another value is specified. We therefore consider the numerical scheme defined by Eq.(36) with flux (39) on the two arcs, conditions (44) - (45) at the extremities of the network and conditions (48) at the junction; this scheme will be referred as the HLL-(48) scheme in the following.

We consider a uniform spatial grid with a fixed spatial step $\Delta x = 0.05$ on the two arcs with equal length of $L_\ell = L_r = 2$. Then, the number of cells verify $J_\ell = J_r = J$. The time step is dynamically computed at each time iteration n by the CFL condition

$$\Delta t^n \leq \frac{\Delta x}{\max\{\lambda_\ell^n, \lambda_r^n\}},$$

where λ_ℓ^n and λ_r^n have been defined in Proposition 4.2, such that the subcharacteristic condition (57) is verified.

5.1. **Numerical convergence results for the numerical scheme HLL-**(48)**.** Let the following Gaussian function be given

$$g(x;\sigma,c) = e^{-(x-c)^2/2\sigma^2}.$$

To study the numerical order of convergence of the scheme applied to the whole network, we set as initial data (at time $t = 0$), on the left arc, for $x\in[0, L_\ell]$,

$$\rho_\ell(0,x) = 1.5 + g(x, 0.2, 0.8) \text{ and } q_\ell(0,x) = 0.5, \tag{58}$$

and on the right-arc, for $x \in [0, L_r]$,

$$\rho_r(0,x) = 1 + g(x, 0.1, 0.5) \text{ and } q_r(0,x) = 0.5. \tag{59}$$

This initial condition is subsonic all over the network and verifies at the junction the continuity of the flux and the (JTC) condition (3) with $\kappa = 1$, i.e.

$$q_\ell(0, L_\ell) = q_r(0,0) = \rho_\ell(0, L_\ell) - \rho_r(0,0) = 0.5.$$

The accuracy is measured by the L^1 norm of the error at the final time $T = 1$, defined as

$$\text{err}_{\rho,\ell} = \Delta x \sum_{j=1}^{J_\ell} |\rho_{j,\ell}^N - \rho_{j,\ell}^{ref}|, \quad \text{err}_{q,\ell} = \Delta x \sum_{j=1}^{J_\ell} |q_{j,\ell}^N - q_{j,\ell}^{ref}|,$$

with the same definition for arc r, where $(\rho_\cdot^{ref}, q_\cdot^{ref})$ is a reference solution obtained with a small $\Delta x \sim 10^{-5}$ on both arcs ℓ and r. Considering the system (48) at the junction, Table 1 shows that the conditions imposed at the junction do not affect the convergence order of the scheme, which remains first order.

Furthermore, we show that the system (48) does not alter the asymptotic behavior of the solution along the entire 2-arc network. We consider again the initial data (58)–(59) and calculate the rate of convergence of the solution to the expected asymptotic state

$$\bar\rho_{asympt} = \frac{1}{L_\ell + L_r} \int_0^{L_\ell + L_r} (\rho_\ell(0,x) + \rho_r(0,x))\, dx, \ \bar q_{asympt} = 0. \tag{60}$$

Given N data points $(t_i, e_{\rho,\ell}(t_i))_{i=1,\cdots,N}$, we shall define γ and C as the solution of the following least square problem,

$$\min_{C,\gamma} \sum_{i=1}^{N} |\ln(e_{\rho,\ell}(t_i)) - \ln(C\, t_i^{-\gamma})|^2, \tag{61}$$

where $e_{\rho,\ell}(t_i) = \|\rho_\ell(t_i,\cdot) - \bar\rho_{asympt}\|_{L^1,L^\infty}$, with the same definition for $e_{\rho,r}$, $e_{q,\ell}$ and $e_{q,r}$. Table 2 presents the optimal values of γ and C. Once again, the system imposed at the junction does not alter the asymptotic behavior in time of the solution, see [35], where it is proved that the solution decays as t^{-1}, in the case of a single interval.

	ρ_ℓ		ρ_r		q_ℓ		q_r	
Δx	$\text{err}_{\rho,\ell}$	order	$\text{err}_{\rho,r}$	order	$\text{err}_{q,\ell}$	order	$\text{err}_{q,r}$	order
0.0063	0.02651	0.70286	0.04090	0.81492	0.05104	0.77079	0.06378	0.63251
0.0031	0.01495	0.82633	0.02151	0.92712	0.02727	0.90406	0.03558	0.84207
0.0016	0.00743	1.00890	0.01030	1.06292	0.01407	0.95527	0.01742	1.02998
0.0008	0.00334	1.15396	0.00453	1.18482	0.00655	1.10264	0.00775	1.16828

TABLE 1. L^1 error and order of convergence of the numerical scheme HLL-(48) on both arcs starting from the regular initial data (58)–(59).

	ρ_ℓ		ρ_r		q_ℓ		q_r	
	C	γ	C	γ	C	γ	C	γ
L^1	0.2356	1.0248	0.2301	1.0274	0.5642	0.9802	0.5193	0.9544
L^∞	0.2295	1.0558	0.2295	1.0558	0.5662	1.0493	0.5446	1.0371

TABLE 2. Optimal values of γ and C given by the least square problem (61) with $e_{\rho,\ell}(t_i) = \|\rho_\ell(t_i,\cdot) - \bar{\rho}_{asympt}\|_{L^1,L^\infty}$ for $i = 1,\dots,N$ computed in L^1 and L^∞ norms, same definition for $e_{\rho,r}$, $e_{q,\ell}$ and $e_{q,r}$.

5.2. **Comparison between the two numerical schemes HLL-**(48) **and HLL-**(28)**.** Now, we also consider the so-called HLL-(28) scheme, which is defined as the previous HLL-(48) scheme, unlike the junction condition which is taken here as the solution of system (28) defined at Sec.3 thanks to Riemann invariant considerations.

In this section we compare the dynamics obtained by the two schemes HLL-(48) and HLL-(28), examining the subsonic and supersonic cases. In all tests, we start from data verifying condition (3) with $\kappa = 1$ at the junction, i.e.

$$q_\ell(0,L_\ell) = q_r(0,0) = \rho_\ell(0,L_\ell) - \rho_r(0,0).$$

In the following figures, these initial data are drawn in dashed black lines.

We consider the following test problems:

Test C1: Case of a subsonic initial datum, constant on both arcs,

$$\begin{cases} \rho_\ell(0,x) = 4.5, & q_\ell(0,x) = 0.5, \quad \text{for all } x \in [0,L_\ell], \\ \rho_r(0,x) = 4, & q_r(0,x) = 0.5, \quad \text{for all } x \in [0,L_r]. \end{cases}$$

As can be seen in Figure 5, the two schemes HLL-(48) and HLL-(28) give qualitatively the same results on both arcs and the junction. We also notice that solutions are converging in large times to the asymptotic constant state described at Eq.(60).

Test C2: Case of a non constant initial datum given by

$$\begin{cases} \rho_\ell(0,x) = 0.4 + g(x,0.2,0.8) & \text{and} \quad q_\ell(0,x) = 0.1, \quad \text{for all } x \in [0,L_\ell], \\ \rho_r(0,x) = 0.3 + g(x,0.1,0.5) & \text{and} \quad q_r(0,x) = 0.1, \quad \text{for all } x \in [0,L_r], \end{cases}$$

which is subsonic at the junction. As can be seen in Figure 6, the two approaches show some differences in the calculated values at the junction (look particularly at Figure 6-(a) at time $T/4$), but these do not propagate along the arcs and vanish over time. Here again the solutions converge to the expected asymptotic profile for large times.

Test C3: Case of a constant initial datum supersonic to the right of the junction (right-arc) and subsonic on the left,

$$\begin{cases} \rho_\ell(0,x) = 2.5, & q_\ell(0,x) = 0.5, \quad \text{for all } x \in [0,L_\ell], \\ \rho_r(0,x) = 2, & q_r(0,x) = 0.5, \quad \text{for all } x \in [0,L_r]. \end{cases}$$

As can be seen in Figure 7, on the right arc the solution at the junction remains supersonic and the two algorithms give the same results. This is an example where the datum on the right is supersonic but with positive velocity, namely $q_r(0,L_r) > 0$ and $q_r(0,L_r) > q_s^+(\rho_r(0,L_r))$. In this case, the Riemann based HLL-(28) scheme selects the solution on the right invariant curve, see Subsec.3.3, and so does the HLL-(48) scheme .

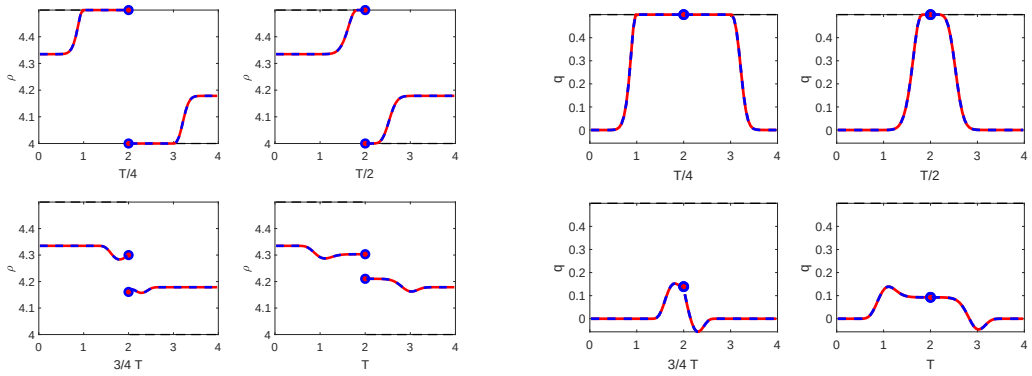

(a) Function ρ (b) Function q

FIGURE 5. **Test C1**. Comparison of the solutions given by scheme HLL-(48) (in solid red line) and by scheme HLL-(28) (in dashed blue line), starting from a constant subsonic initial datum on both arcs. The blue and red dots represent the values at the junction. On the left, function ρ and on the right, function q for different times $t = 0.25$, 0.5 and 0.75 with final time $T = 1$.

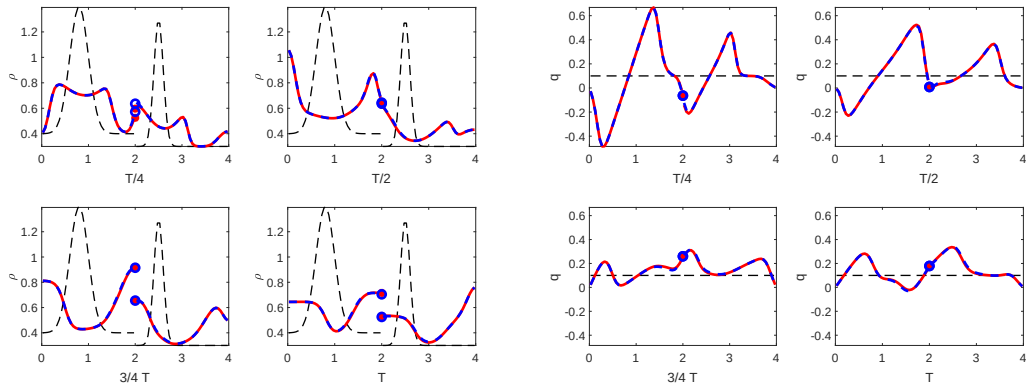

(a) Function ρ (b) Function q

FIGURE 6. **Test C2**. Comparison of the solutions given by scheme HLL-(48) (in solid red line) and by scheme HLL-(28) (in dashed blue line), starting from a subsonic non constant initial datum (in dashed black line). The blue and red dots represent the values at the junction. On the left, function ρ and on the right, function q for different times $t = 0.25$, 0.5 and 0.75 with final time $T = 1$.

Test C4: Case of a non constant initial datum given by

$$\begin{cases} \rho_\ell(0,x) = 0.1 + g(x, 0.2, 0.8) & \text{and} \quad q_\ell(0,x) = -0.2, \quad \text{for all } x \in [0, L_\ell], \\ \rho_r(0,x) = 0.3 + g(x, 0.1, 0.5) & \text{and} \quad q_r(0,x) = -0.2, \quad \text{for all } x \in [0, L_r], \end{cases}$$

which is supersonic to the left of the junction (left-arc) and subsonic to the right of the junction. As can be seen in Figure 8, the two methods produce different results,

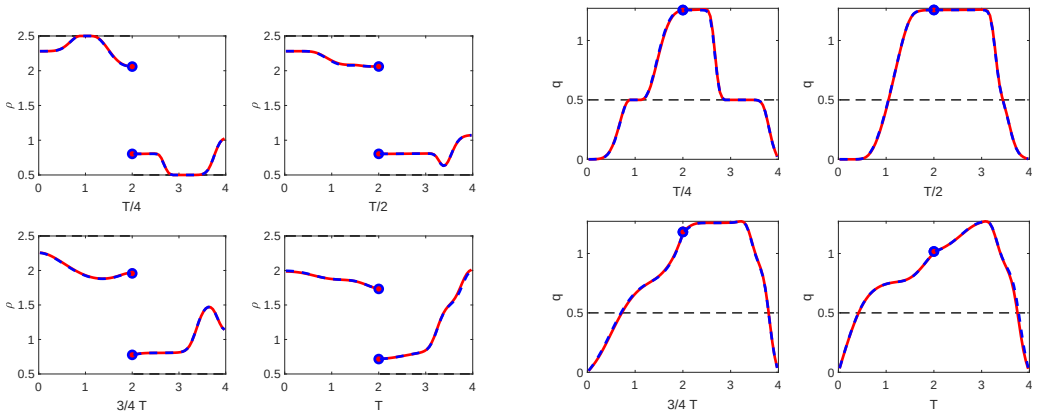

(a) Function ρ (b) Function q

FIGURE 7. **Test C3**. Comparison of the solutions given by scheme HLL-(48) (in solid red line) and by scheme HLL-(28) (in dashed blue line), starting from a constant initial datum supersonic on the right-arc and subsonic on the left-arc. The blue and red dots represent the values at the junction and the dashed black line the initial value for q. On the left, function ρ and on the right, function q for different times $t = 0.25$, 0.5 and 0.75 with final time $T = 1$.

particularly on the left arc. This is even more visible in Figure 9, where we plot the evolution in time of the four junction values ρ_ℓ^*, ρ_r^*, q_ℓ^* and q_r^*. We observe, on the left arc the flow transition from the supersonic region to the subsonic one, and that the two solvers, HLL-(48) and HLL-(28), produce some slightly different results, especially before the transition. This is an example where the datum on the left is supersonic with negative velocity, namely $q_\ell(0, L_\ell) < 0$ and $q_\ell(0, L_\ell) < q_s^-(\rho_\ell(0, L_\ell))$. In this case the Riemann based algorithm selects the solution on the right invariant curve, see Subsection 3.3, while the relaxation one (48) gives a result which is not quite the same.

5.3. **Study of different values for parameter κ.** In this test case, we show the numerical dynamics obtained by scheme HLL-(48) for two different values of parameter κ. We assume a constant initial datum given by

$$\begin{cases} \rho_\ell(0, x) = 2.5, & \text{for all } x \in [0, L_\ell], \\ \rho_r(0, x) = 0.5, & \text{for all } x \in [0, L_r], \end{cases}$$

and

$$q_\ell(0, x) = q_r(0, x) = \kappa(\rho_\ell(0, x) - \rho_r(0, x)) = 2\kappa.$$

In Figure 10, we show the density evolution obtained with the two values $\kappa = 100$ and $\kappa = 0.1$.

On the one hand, as expected, for $\kappa = 100$ the density values at the junction start out different and then tend to converge until they coincide. This is coherent since for large values for κ, we expect the system to behave similarly to the system with the continuity of densities at the junction, that is to say the junction condition that is usually considered in other articles. On the other hand, for small value of $\kappa = 0.1$, the density remains discontinuous at the interface.

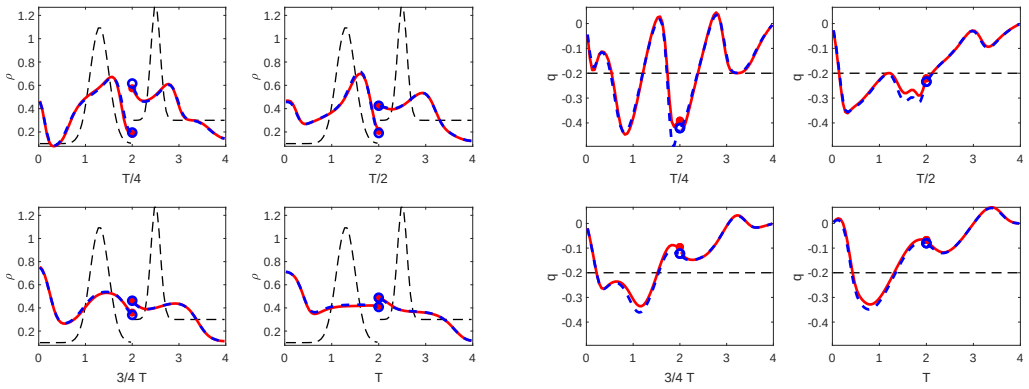

(a) Function ρ (b) Function q

FIGURE 8. **Test C4**. Comparison of the solutions given by scheme HLL-(48) (in solid red line) and by scheme HLL-(28) (in dashed blue line), starting from a non-constant initial datum supersonic on the left-arc and subsonic on the left-arc (in dashed black line). The blue and red dots represent the values at the junction. On the left, function ρ and on the right, function q for different times $t = 0.25$, 0.5 and 0.75 with final time $T = 1$.

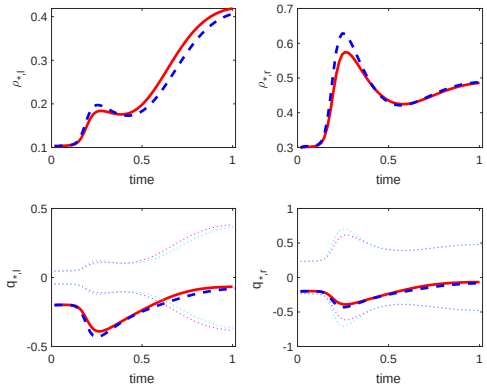

FIGURE 9. **Test C4**. Evolution with respect to time of the 4 junction values: $\rho_{*,\ell}$ on the top left subfigure, $\rho_{*,r}$ on the top right, $q_{*,\ell}$ on the bottom left and $q_{*,r}$ on the bottom right, computed by scheme HLL-(48) (in solid red line) and by scheme HLL-(28) (in dashed blue line). The two dotted lines in the figures on the bottom delineate the boundary between the subsonic and supersonic regions (the sonic curve given for the corresponding value of ρ), in pink for the HLL-(48) scheme and in light blue for the HLL-(28) scheme. The regime is subsonic inside these two curves and supersonic outside.

Note that the Riemann-based HLL-(28) scheme does not provide a solution to test case with $\kappa = 100$, whereas scheme HLL-(48) does; it would be necessary to expand the region of admissible solutions and add further conditions to uniquely define the unknown values at the junction.

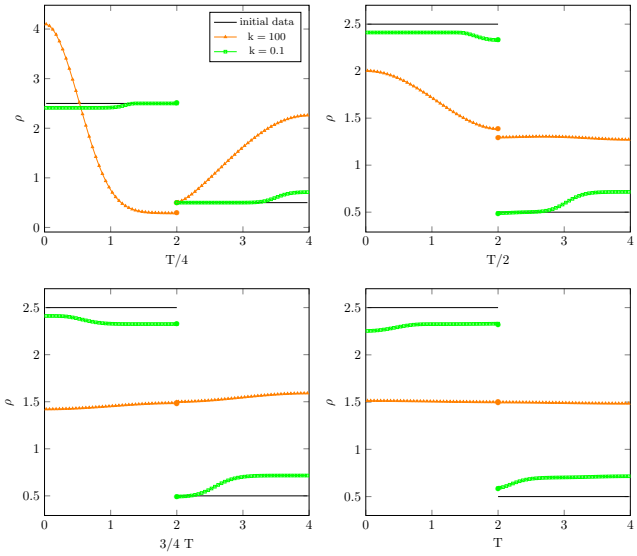

FIGURE 10. **Different values for parameter κ.** Density solution obtained with the approximation HLL-(48), starting from a constant initial datum on both arcs (in solid black line), for two different values of parameter κ : $\kappa = 100$ (dotted orange line) and $\kappa = 0.1$ (dotted green line), for different times $t = 0.5$, 1 and 1.5 with final time $T = 2$.

5.4. **Entropy dissipation at the discrete level.** In this subsection, following the discussion in Section 2, we investigate the evolution of the total entropy in the network,

$$S(t) = \int_0^{L_\ell + L_r} \eta(\rho(t,x), q(t,x))dx \approx S^n = \Delta x \sum_{j=0}^{J_\ell + J_r} \eta_j^n, \tag{62}$$

where η is the entropy function defined in (17) and $\eta_j^n = \eta(\rho_j^n, q_j^n)$ for j running along the nodes of the two arcs forming the network. We are unable to prove analytically the entropy decay for the numerical scheme, but our numerical experiments show that the decay is better in the numerical case than what is expected at the continuous level.

We assume two different constant initial data which verify (3) :

$$q_\ell(0,x) = q_r(0,x) = \kappa(\rho_\ell(0,x) - \rho_r(0,x)),$$

with $\kappa = 1$, and which differ in the amplitude of the density jump at the junction:

(E1) $\rho_\ell(0,x) = 1.5$ and $\rho_r(0,x) = 1$ such that $q_\ell(0,x) = q_r(0,x) = \rho_\ell(0,x) - \rho_r(0,x) = 0.5$.
(E2) $\rho_\ell(0,x) = 6$ and $\rho_r(0,x) = 1$ such that $q_\ell(0,x) = q_r(0,x) = \rho_\ell(0,x) - \rho_r(0,x) = 5$.

We recall here the entropy dissipation inequality (19) : $S(t) \leq S(0) - \int_0^t \Delta G(s)ds$.

As can be seen in Figure 11-(right) and Figure 12-(right), for both initial data the total entropy (62) is decreasing in time and numerically verify a discrete version of the inequality (19), i.e.

$$S^n = \Delta x \sum_{j=0}^{J_\ell+J_r} \eta_j^n \leq \Delta x \sum_{j=0}^{J_\ell+J_r} \eta_j^0 - \Delta t \sum_{k=0}^{n} \left(G_\ell^{*,k} - G_r^{*,k} \right) = S^0 - \Delta t \sum_{k=0}^{n} \Delta G^{*,k}, \tag{63}$$

where $G_\ell^{*,n} = G(\rho_\ell^{*,n}, q_\ell^{*,n})$ and $G_r^{*,n} = G(\rho_r^{*,n}, q_r^{*,n})$ represent the values of the entropy flux, as defined in (17), computed at the left and right junction states obtained from the solution of system (48) at time step n. As in Section 2, we also define the quantity $\Delta G^{*,n} := G_\ell^{*,n} - G_r^{*,n}$, which is a discrete version at time t_n of quantity ΔG.

Specifically, for the small jump assumed in test case (E1), the quantity ΔG, displayed in Figure 11-(a), continuous line, is positive for all time $t > 0$ as expected from the discussion in Section 2, thus ensuring the dissipation of entropy with respect to time. We notice in Figure 11-(b) that the estimate $S(0) - \displaystyle\int_0^t \Delta G(s) ds$ is above the entropy for all times, as expected, and is equal up to a constant to the integral displayed on Figure 11-(a). We also observe that in that case the estimate is sharp.

However, for big density jumps at the junction, like in test case (E2), the variation $\Delta G(t)$ is negative for all times, as displayed in Figure 12-(a), continuous line. But, even if the right hand part of the inequality (63) is increasing, and the bound from above $S(0) - \displaystyle\int_0^t \Delta G(s) ds$ is therefore not accurate, the total entropy remains decreasing in time, see Figure 12-(b). We can interpret this as follows : the dissipation of entropy along the arcs is large enough to compensate the small enough non-dissipation of entropy at the junction.

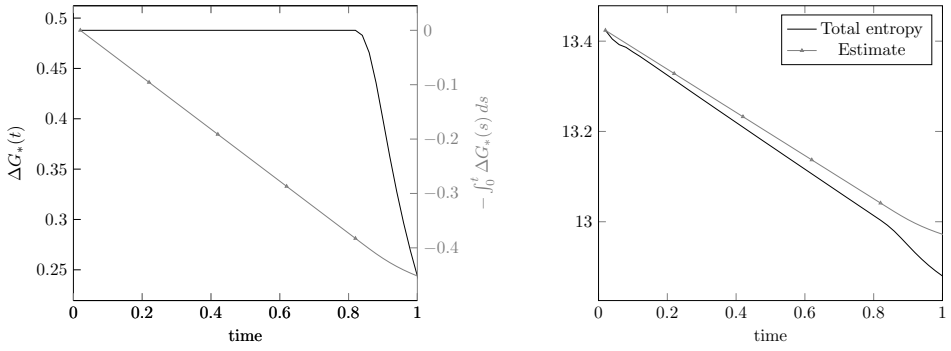

(a) (b)

FIGURE 11. **Entropy dissipation**, test case (E1), small jump at the junction. (a) Plot of ΔG with respect to time (solide black line and range of values on the left) and of $-\int_0^t \Delta G(s)\, ds$ (dotted grey line and range of values on the right). (b) Plot of the total entropy S (solid black line) as a function of time and of the right hand side $S(0) - \displaystyle\int_0^t \Delta G(s) ds$ of inequality (63) (dotted grey line).

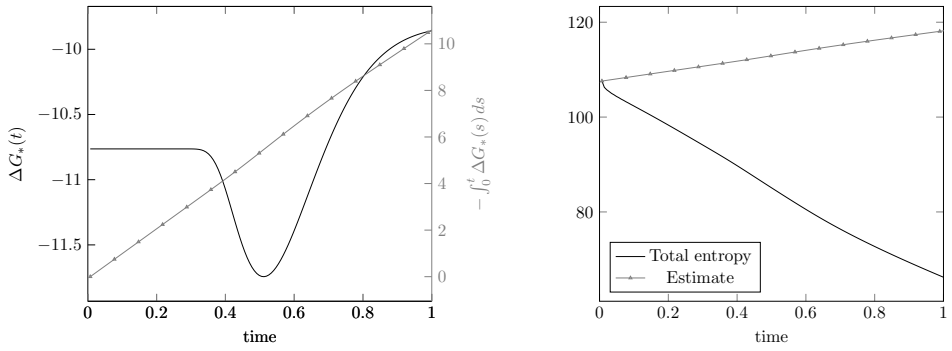

(a) (b)

FIGURE 12. **Entropy dissipation**, test case (E2), large jump at the junction. (a) Plot of ΔG with respect to time (solide black line and range of values on the left) and of $-\int_0^t \Delta G(s)\,ds$ (dotted grey line and range of values on the right). (b) Plot of the total entropy S (solid black line) as a function of time and of the right hand side $S(0) - \displaystyle\int_0^t \Delta G(s)ds$ of inequality (63) (dotted grey line).

5.5. **Simulations in the case $\gamma = 4/3$.** To conclude this part of the numerical tests, let us consider the problem with a different value of γ in the pressure law (2). We take $\gamma = 4/3$ and the constant initial datum (same as (E2)) given by

$$\begin{cases} \rho_\ell(0,x) = 6, \quad q_\ell(0,x) = 5, & \text{for all } x \in [0, L_\ell], \\ \rho_r(0,x) = 1, \quad q_r(0,x) = 5, & \text{for all } x \in [0, L_r]. \end{cases}$$

Note that here the simulations are performed using only the scheme HLL-(48), since the scheme HLL-(28) is not able to handle this case (there is no simple solution to the corresponding Riemann problem).

The results are shown in Figure 13. We notice first that the evolution is much slower than in the case $\gamma = 2$ and that function q is decreasing towards 0 but very slowly. We also observe that before going asymptotically towards a constant state, the density ρ tends to form a bump like solution on the right arc of the network, see the function ρ at different times on the left subfigure.

To offer a comprehensive overview, we add a final test to compare HLL-(48) and HLL-(28) when $\gamma \neq 2$. We set $\gamma = 4/3$ and consider the subsonic setting of Test C2. As can be seen in Figure 14, we obtain a similar result to that for $\gamma = 2$ in Figure 6: the two approaches produce different calculated values at the junction, but these differences do not propagate along arcs and disappear over time.

6. Extensions to a general network

To begin with, we consider an extension of what has been previously done to more complicated network, i.e. networks with any number of arcs where nodes can be connected to any number of arcs.

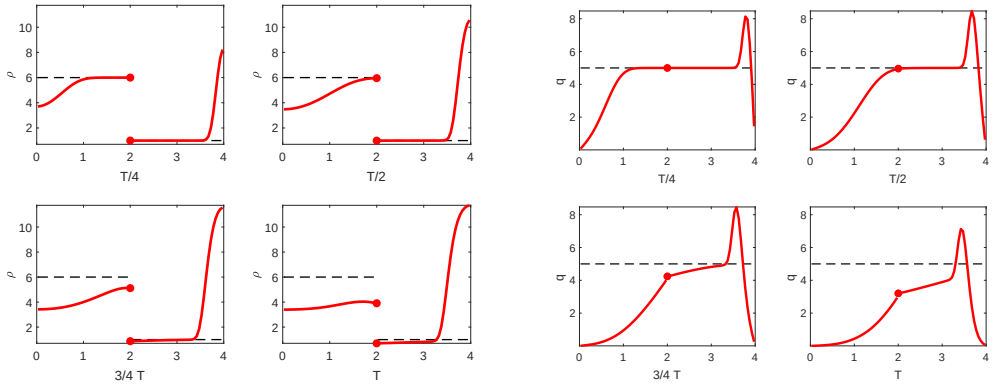

(a) Function ρ (b) Function q

FIGURE 13. **Simulation for** $\gamma = 4/3$. Solutions given by scheme HLL-(48) (in solid red line), starting from a constant initial datum (in dashed black line) on both arcs. The red dots represent the values at the junction. On the left, function ρ and on the right, function q for different times $t = 0.25$, 0.5 and 0.75 with final time $T = 1$.

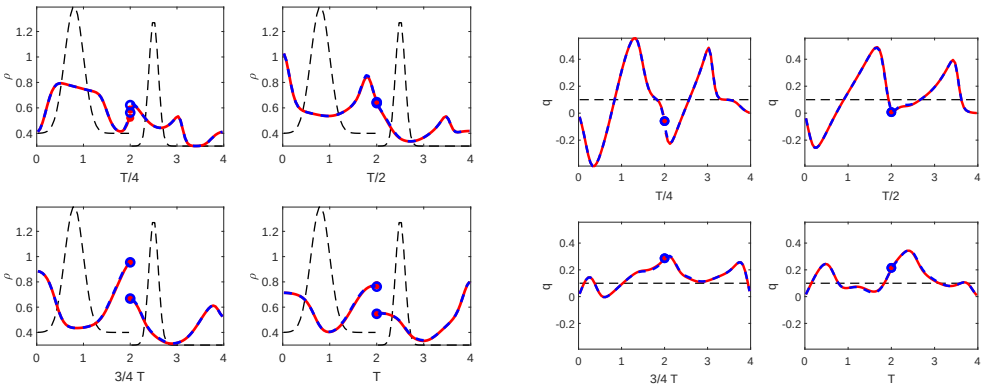

(a) Function ρ (b) Function q

FIGURE 14. **Simulation for** $\gamma = 4/3$. Comparison of the solutions given by scheme HLL-(48) (in solid red line) and by scheme HLL-(28) (in dashed blue line), starting from the subsonic non constant initial datum (in dashed black line) given in Test C2. The blue and red dots represent the values at the junction. On the left, function ρ and on the right, function q for different times $t = 0.25$, 0.5 and 0.75 with final time $T = 1$.

Let us define a network or a connected graph $G = (\mathcal{N}, \mathcal{A})$, as composed of two finite sets, a set of nodes (or vertices) $\mathcal{N}$ and a set of N arcs $\mathcal{A}$, such that an arc connects a pair of nodes. Since arcs are bidirectional the graph is non-oriented, but we need to fix an artificial orientation in order to fix a sign to the velocities. The network is therefore composed of "oriented" arcs

and there are two different types of intervals at a node $p \in \mathcal{N}$: incoming ones – the set of these intervals is denoted by $\mathcal{I}_p$ – and outgoing ones – whose set is denoted by $\mathcal{O}_p$. See, for example, Figure 15 for the representation of a 4-arc and 1node -network, with 2 incoming arcs and 2 outgoing arcs, where $1, 2 \in \mathcal{I}_1$ and $3, 4 \in \mathcal{O}_1$.

6.1. **Extension of junction conditions** (53)**.** Let us consider now a node $p \in \mathcal{N}$, which is the junction of N_p arcs, denoted by i, with $1 \leq i \leq N_p$. We denote by $\mathcal{I}_p$ the set of incoming arcs and by $\mathcal{O}_p$ the set of outgoing arcs.

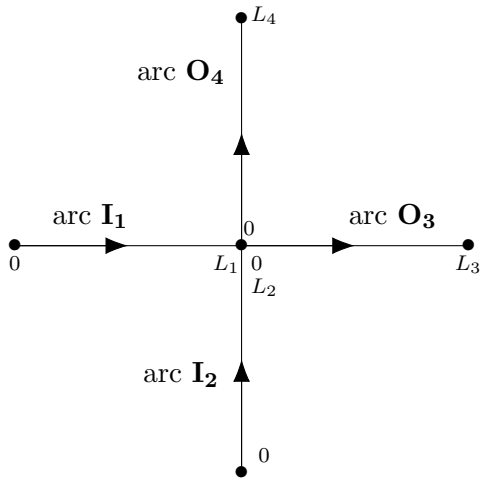

FIGURE 15. An example of a 4 arc network with 2 incoming arcs and 2 outgoing arcs

We will first generalize at the continuous level conditions (13) for the outer nodes and then conditions (3) for junction nodes. Then, we give a numerical discretization of these conditions, namely a generalization of discrete conditions (44)- (45) on outer nodes and conditions (53) at junction nodes. Note that the "discrete equality junction conditions" (53) are straightforward to generalize unlike Riemann invariant junction conditions (28), which would be much more involved to consider for general networks.

Therefore, the generalization of conditions (13) **at all outer nodes, i.e. non-junction nodes** reads as :

$$\begin{cases} \partial_x \rho_i(\cdot, L_i) = 0 \text{ and } q_i(\cdot, L_i) = 0, & \text{if } i \in \mathcal{O}_p, \\ \partial_x \rho_i(\cdot, 0) = 0 \text{ and } q_i(\cdot, 0) = 0. & \text{if } i \in \mathcal{I}_p, \end{cases} \tag{64}$$

We now consider the generalization of conditions (3) **at all inner nodes, i.e. junction nodes.** At the junction node $p \in \mathcal{N}$, we set the following conditions, which say that the flux is equal to a linear combination of the different differences of densities on the various arcs :

$$\begin{cases} -q_i(\cdot, 0) = \sum\limits_{j \in \mathcal{I}_p} \kappa_{i,j}(\rho_i(\cdot, 0) - \rho_j(\cdot, L_j)) + \sum\limits_{j \in \mathcal{O}_p} \kappa_{i,j}(\rho_i(\cdot, 0) - \rho_j(\cdot, 0)) & \text{if } i \in \mathcal{O}_p, \\ q_i(\cdot, L_i) = \sum\limits_{j \in \mathcal{I}_p} \kappa_{i,j}(\rho_i(\cdot, L_i) - \rho_j(\cdot, L_j)) + \sum\limits_{j \in \mathcal{O}_p} \kappa_{i,j}(\rho_i(\cdot, L_i) - \rho_j(\cdot, 0)) & \text{if } i \in \mathcal{I}_p, \end{cases} \tag{65}$$

where $\kappa_{i,j} \geq 0$ are generalizations of permeability coefficients between two arcs.

In order to have the mass conservation property at the junction $p \in \mathcal{N}$, we also impose a generalization of condition (15), which reads as :

$$\sum_{i\in\mathcal{O}_p} -q_i(\cdot,0) + \sum_{i\in\mathcal{I}_p} q_i(\cdot,L_i) = 0. \tag{66}$$

If we impose that the transmission coefficients are symmetric, namely

$$\kappa_{i,j} = \kappa_{j,i},$$

condition (66) is automatically satisfied. This condition ensures that the total mass of the whole system is conserved, namely

$$\frac{d}{dt}m(t) = 0, \text{ with } m(t) = \sum_{i\in\mathcal{A}} \int_0^{L_i} \rho_i(t,x)\,dx. \tag{67}$$

Now, let us consider the discretization of the previous conditions on the outer nodes and at the junction, following the ideas of Sec.4.

For the outer nodes, we set, in the spirit of conditions (44)- (45) :

$$\begin{cases} \rho_{0,i} = \rho_{1,i} \text{ and } q_{0,i} = -q_{1,i} & \text{if } i \in \mathcal{O}_p, \\ \rho_{J_i,i} = \rho_{J_i-1,i} \text{ and } q_{J_i,i} = -q_{J_i-1,i} & \text{if } i \in \mathcal{I}_p. \end{cases} \tag{68}$$

Now, at each node $p \in \mathcal{N}$, we will need to solve a linear system. Namely, at node $p \in \mathcal{N}$, considering the junction conditions with N_p arcs, we need to compute $2N_p$ values, that we denote ρ_i^* and q_i^* for $1 \le i \le N_p$. Equations (65) give at the discrete level the following N_p equations :

$$\begin{cases} -q_i^* = \displaystyle\sum_{j\in\mathcal{I}_p} \kappa_{i,j}(\rho_i^* - \rho_j^*) + \sum_{j\in\mathcal{O}_p} \kappa_{i,j}(\rho_i^* - \rho_j^*) & \text{if } i \in \mathcal{O}_p, \\ q_i^* = \displaystyle\sum_{j\in\mathcal{I}_p} \kappa_{i,j}(\rho_i^* - \rho_j^*) + \sum_{j\in\mathcal{O}_p} \kappa_{i,j}(\rho_i^* - \rho_j^*) & \text{if } i \in \mathcal{I}_p. \end{cases} \tag{69}$$

We obtain N_p other equations by imposing a generalization of equation (51) :

$$\begin{cases} \mathcal{F}^\rho(U_{1,i}, U_i^*) = q_i^*, & \text{if } i \in \mathcal{O}_p, \\ \mathcal{F}^\rho(U_{J_i,i}, U_i^*) = q_i^* & \text{if } i \in \mathcal{I}_p. \end{cases} \tag{70}$$

In the case of the HLL flux, the system (70) becomes

$$\begin{cases} \dfrac{q_i^* + q_{1,i}}{2} + \dfrac{\lambda_i}{2}(\rho_i^* - \rho_{1,i}) = q_i^*, & \text{if } i \in \mathcal{O}_p, \\ \dfrac{q_i^* + q_{J_i,i}}{2} - \dfrac{\lambda_i}{2}(\rho_i^* - \rho_{J_i,i}) = q_i^* & \text{if } i \in \mathcal{I}_p. \end{cases}$$

or equivalently

$$\begin{cases} q_i^* = q_{1,i} + \lambda_i(\rho_i^* - \rho_{1,i}), & \text{if } i \in \mathcal{O}_p, \\ q_i^* = q_{J_i,i} - \mu_i(\rho_i^* - \rho_{J_i,i}), & \text{if } i \in \mathcal{I}_p. \end{cases} \tag{71}$$

Combining Eq.(71) and (69), we obtain the following system composed of N_p equations :

$$\begin{cases} \displaystyle\sum_{j\in\mathcal{I}_p} \kappa_{i,j}(\rho_i^* - \rho_j^*) + \sum_{j\in\mathcal{O}_p} \kappa_{i,j}(\rho_i^* - \rho_j^*) + \mu_i\rho_i^* = -q_{1,i} + \mu_i\rho_{1,i} & \text{if } i \in \mathcal{O}_p, \\ \displaystyle\sum_{j\in\mathcal{I}_p} \kappa_{i,j}(\rho_i^* - \rho_j^*) + \sum_{j\in\mathcal{O}_p} \kappa_{i,j}(\rho_i^* - \rho_j^*) + \mu_i\rho_i^* = q_{J_i,i} + \mu_i\rho_{J_i,i} & \text{if } i \in \mathcal{I}_p. \end{cases} \tag{72}$$

Therefore, at node $p \in \mathcal{N}$, the vector $(\rho_1^*, \cdots, \rho_{N_p}^*)$ is solution to a linear system, which is invertible, as soon as $\kappa_{i,j} \geq 0$ and $\mu_i > 0$, since the matrix

$$\begin{pmatrix} \sum_{j\neq 1} \kappa_{1,j} + \mu_1 & & & \\ & \ddots & & -\kappa_{i,j} \\ & & \ddots & \\ -\kappa_{i,j} & & & \sum_{j\neq N_p} \kappa_{N_p,j} + \mu_{N_p} \end{pmatrix}, \tag{73}$$

is a strictly diagonally dominant matrix. Values for momenta q_i^*, $1 \leq i \leq N_p$ are then given by Eq.(71).

6.2. **Properties of the numerical scheme.** It is now easy to generalize the mass conservation and the positivity of solution, already demonstrated at Sec.4.4 in the case of a 2 arc network, to the case of a N arc network. However, the entropy dissipation property is far more complicated and will not be treated here. First, we prove the following property, which is equivalent to the continuous mass preservation (67).

Proposition 6.1. *Let us consider system* (11) *set on a N-arc network with boundary conditions* (64) *on the outer nodes and junction conditions* (65) *with symmetric coefficients, that is to say $\kappa_{i,j} = \kappa_{j,i}$. The numerical scheme* (36) *with discrete boundary conditions* (68) *on the outer nodes and discrete junction conditions* (69) *is mass-preserving, that is to say the discrete mass $m_{tot}^n = h \sum_{i=1}^{N} \sum_{j=1}^{J_i} \rho_{j,i}^n$ is independent of $n \in \mathbb{N}$.*

Proof. We consider the first component of equation (36). The conservation of mass is given by Eq.(68) and (69) with $\kappa_{i,j} = \kappa_{j,i}$, which leads to

$$\sum_{i\in\mathcal{O}_p} -q_i^* + \sum_{i\in\mathcal{I}_p} q_i^* = 0.$$

□

Now, we prove the generalization of the positivity of the solution in the particular case of HLL numerical flux :

Proposition 6.2. *Let us consider scheme* (36) *with flux* (40) *on a N arc network, boundary conditions* (68) *and conditions* (69)-(70) *at the junction in order to discretize system* (11)-(64)-(65) *on a general network. We define $\lambda_i^n > 0$ such that*

$$\lambda_i^n \geq \max_{1\leq j\leq J_i} |u_{j,i}^n| + \sqrt{p'(\rho_{j,i}^n)}, \text{ for } 1 \leq i \leq N.$$

If the initial condition is positive, that is to say

$$\rho_{j,i}^0 \geq 0 \text{ for all } 1 \leq i \leq N, \text{ for all } 1 \leq j \leq J_i,$$

then the solution remains positive in time, that is to say

$$\rho_{j,i}^n \geq 0 \text{ for all } 1 \leq i \leq N, \text{ for all } 1 \leq j \leq J_i, \text{ for all } n \in \mathbb{N}.$$

Proof. We prove the proposition by induction, following the proof of Prop.4.2. Assume that $\rho_{j,i}^n \geq 0$ for all $1 \leq i \leq N$, $1 \leq j \leq J_i$.

We consider node $p \in \mathcal{N}$. Since $\lambda_i^n \geq |u_{j,i}^n|$ for all $1 \leq j \leq J_i$, we can show that the components of the second member of linear system (72) are nonnegative. Moreover, since $\kappa_{i,j} \geq 0$ and $\mu_i^n > 0$, it can be proved easily that the matrix (73) of linear system (72) is a monotone matrix. Consequently the solution $(\rho_1^*, \cdots, \rho_{N_p}^*)$ has positive components and therefore, we can deduce that $\rho_{j,i}^{n+1} \geq 0$ for all $1 \leq i \leq N$, $1 \leq j \leq J_i$. □

6.3. **Numerical tests.** We present now some numerical tests for a general network.

We consider a grid-shaped network with 26 arcs and 18 nodes, see [15] : 16 junction nodes and 2 outer nodes, see Figure16. The junction nodes are connecting to 2, 3 or 4 arcs, namely nodes inside the grid are connected to 4 nodes, nodes on the arcs of the grid to 3 nodes and nodes on the corners of the grids to 2 or 3 other nodes. Permeability coefficients depend on the number of arcs at the node, more precisely if we denote by N_p the number of arcs at node p, then $\kappa_{i,j} = 1/N_p$ for all $i \neq j$ and 0 otherwise. The lengths of the arcs are also different and are equal to $L = 10$ except $L_1 = L_5 = L_9 = L_{10} = L_{14} = L_{21} = L_{25} = L_{26} = 0.5$. Note that, for readability reasons, we plot on the figures all the arcs with the same length, although different length values are taken in the computation.

The initial density ρ is a small perturbation on each arc of a constant equal to 0.45 and the initial momentum q is constant everywhere equal to 0.1. We let the system evolves until $T = 150$, see Figure 17.

We notice that the system reaches an asymptotic state with some null momentum q on each arc of the network and a constant density ρ which is the same on each arc of the network; the constant density can be computed thanks to mass conservation and the initial mass on the whole network.

At time $T = 10$, we notice that positive values for q are concentrated around the nodes of the network, whereas null or positive values of the momentum take place on the arcs. Regarding the density, we remark the highest values on the arcs around one outer node of the network and the smallest values around the other outer node.

At time $T = 50$, the values for the density follow the same pattern as for $T = 10$, but the values are more homogeneous all around the network. As for the momentum, it is null on each arc and q have positive and negative values around the nodes of the networks, where the main changes occur.

Finally at time $T = 150$, once again, the system converges in large time towards a constant state for ρ and q, but the convergence time is much longer than for the previous test cases, since the network is bigger, see Figure17. The value of the density is slightly higher on the arcs with smaller lengths, see the red path on the figure.

7. Conclusions

This paper presents a comprehensive framework for simulating isentropic gas dynamics on networks with jump transmission conditions at junctions. By introducing a relaxation-based numerical scheme, we provided a robust and mass-conserving method that accommodates discontinuities in density and is applicable to both subsonic and supersonic regimes. The scheme is shown to be accurate, stable, and extendable to general network configurations, even when traditional approaches do not work. Numerical tests confirm the method's effectiveness in capturing complex dynamics and its potential for broad applications in

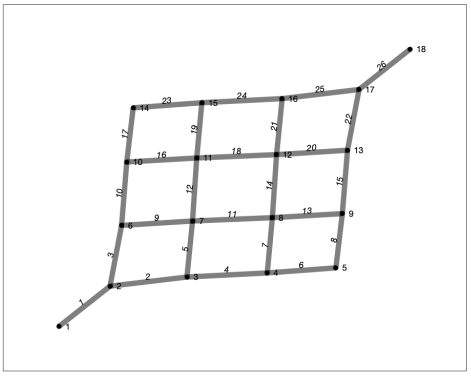

FIGURE 16. Network configuration with 26 arcs and 18 nodes; some of the arcs are smaller

engineering and biological systems. We believe that the relaxation approach can be useful in any situation when the resolution of the exact Riemann problem is not easy to be obtained. Future studies could focus on extending the method to more complex physical models, such as full gas dynamics with additional thermodynamic variables or multi-species flows. The generalization to networks with arbitrary topology and varying transmission coefficients suggests potential applications in modeling biological transport, traffic flow, and energy distribution systems. Analytical challenges remain, particularly in rigorously establishing entropy dissipation for the discrete scheme on large networks and in exploring the uniqueness and stability of solutions under more general transmission conditions.

REFERENCES

[1] B.Andreianov, G.Coclite, C. Donadello, *Well-posedness for vanishing viscosity solutions of scalar conservation laws on a network*, Discrete and Continuous Dynamical Systems, Volume 37, Number 11, 5913-5942 (2017).

[2] D. Aregba-Driollet, *Convergence of lattice Boltzmann methods with overrelaxation for a nonlinear conservation law*, ESAIM, Math. Model. Numer. Anal. 58, No. 5, 1935-1958 (2024).

[3] D. Aregba-Driollet, R. Natalini, *Convergence of relaxation schemes for conservation laws*, Appl. Anal. 61, No. 1-2, 163-190 (1996).

[4] D. Aregba-Driollet, R. Natalini, *Discrete kinetic schemes for multidimensional systems of conservation laws*, SIAM J. Numer. Anal. 37, No. 6, 1973-2004 (2000).

[5] M. K. Banda, M. Herty, and A. Klar, *Coupling conditions for gas networks governed by the isothermal Euler equations. Netw. Heterog. Media*, 1(2):295–314 (electronic), 2006.

[6] G. Bastin, J. Coron, and B. dAndréa Novel, *Using hyperbolic systems of balance laws for modeling, control and stability analysis of physical networks*. In Lecture notes for the Pre-congress workshop on complex embedded and networked control systems, 17th IFAC World Congress, 2008.

[7] F. Bellamoli, L.Müller, E.Toro, *A numerical method for junctions in networks of shallow-water channels*, Appl. Math. Comput., 337, 190-213 (2018).

[8] S. Bianchini, *Hyperbolic limit of the Jin-Xin relaxation model*, Commun. Pure Appl. Math. 59, No. 5, 688-753 (2006).

[9] F. Bouchut, *Construction of BGK models with a family of kinetic entropies for a given system of conservation laws*, J. Stat. Phys. 95, No. 1-2, 113-170 (1999).

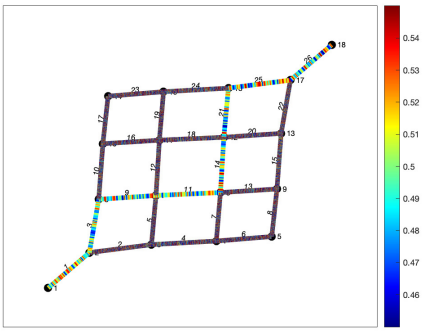

(a) initial condition for ρ

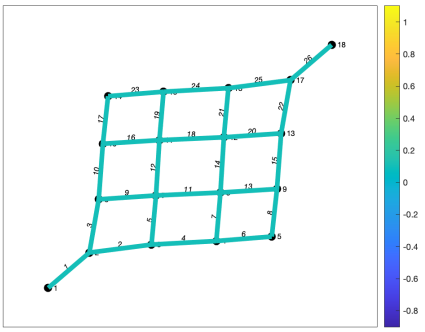

(b) initial condition for q

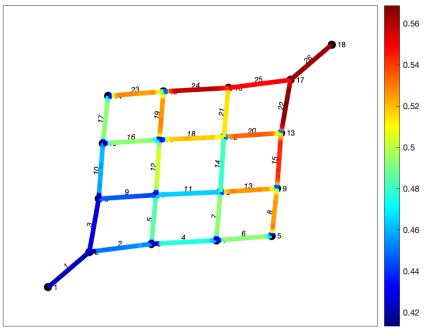

(c) Function ρ at time $T = 10$

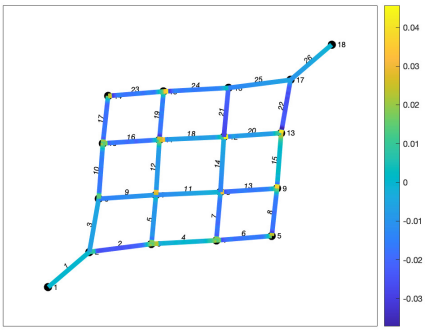

(d) Function q at time $T = 10$

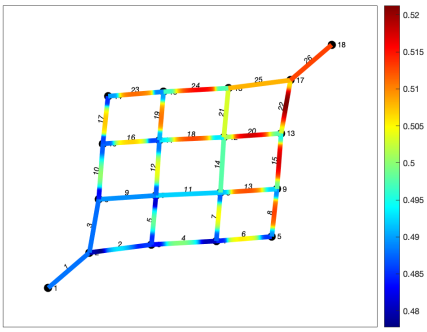

(e) Function ρ at time $T = 50$

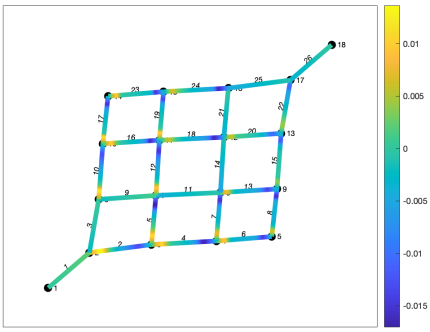

(f) Function q at time $T = 50$

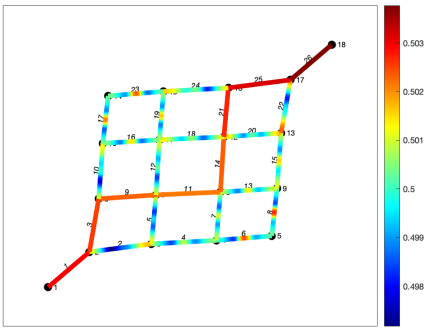

(g) Function ρ at time $T = 150$

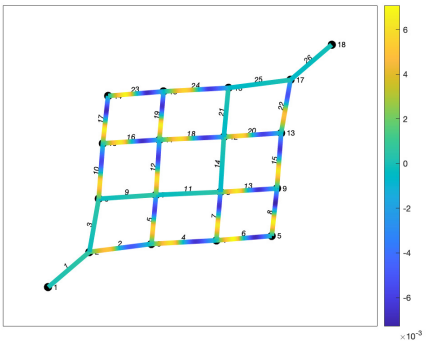

(h) Function q at time $T = 150$

FIGURE 17. Network : on top, initial condition; in the second row, solution at time $T = 10$; in the third row, solution at time $T = 50$; on bottom, solution at time $T = 150$. On the left, function ρ; on the right, function q.

[10] F. Bouchut, Nonlinear stability of finite volume methods for hyperbolic conservation laws and well-balanced schemes for sources. Frontiers in Mathematics. Basel: Birkhäuser (ISBN 3-7643-6665-6/pbk). viii, 135 p. (2004).
[11] A. Bressan; S. Canic; M. Garavello; M. Herty; B. Piccoli, *Flows on networks: Recent results and perspectives*, EMS Surv. Math. Sci., 1, 47-111 (2014).
[12] E. Braun, G. Bretti, and R. Natalini, *Mass-preserving approximation of a chemotaxis multi-domain transmission model for microfluidic chips* Mathematics, 9(6), 2021.
[13] G. Bretti, R. Natalini, and B. Piccoli, *Numerical approximations of a traffic flow model on networks*, Netw. Heterog. Media, 1(1):57–84, 2006.
[14] G. Bretti, R. Natalini, and M. Ribot, *A hyperbolic model of chemotaxis on a network: a numerical study*, ESAIM Math. Model. Numer. Anal., 48(1):231–258, 2014.
[15] G. Bretti, R. Natalini, *Numerical approximation of nonhomogeneous boundary conditions on networks for a hyperbolic system of chemotaxis modeling the Physarum dynamics*, J. Comput. Methods Sci. Eng., 18(1):85–115, 2018.
[16] M. Briani, B. Piccoli, and J.-M. Qiu, *Notes on RKDG methods for shallow-water equations in canal networks*, J. Sci. Comput. 68, 3 (2016), 1101–1123.
[17] M. Briani, B. Piccoli, *Fluvial to torrential phase transition in open canals*, Netw. Heterog. Media 13, No. 4, 663-690 (2018).
[18] M. Briani, G.Puppo, M.Ribot, *Angle dependence in coupling conditions for shallow water equations at channel junctions*, Comput. Math. Appl. 108, 49-65 (2022).
[19] F. Calabrò, P. Zunino, *Analysis of parabolic problems on partitioned domains with nonlinear conditions at the interface: application to mass transfer through semi-permeable membranes*, Mathematical models and methods in applied sciences 16, 4, 479-501 (2006).
[20] A. Cangiani, R. Natalini, *A spatial model of cellular molecular tracking including active transport along microtubules*, Journal of theoretical biology 267, 4, 614-625 (2010).
[21] S. Čanić, E.H. Kim, *Mathematical analysis of the quasilinear effects in a hyperbolic model blood flow through compliant axi-symmetric vessels*, Math. Methods Appl. Sci. 26, No. 14, 1161-1186 (2003).
[22] G. Ciavolella, N. David, A. Poulain, *Effective interface conditions for a porous medium type problem*, Interfaces Free Bound. 26, No. 2, 161-188 (2024).
[23] M. Chaplain, C.Giverso, T.Lorenzi, L.Preziosi, *Derivation and application of effective interface conditions for continuum mechanical models of cell invasion through thin membranes*, SIAM Journal on Applied Mathematics, 79(5), 2011-2031 (2019).
[24] G. Coclite, M. Garavello, *Vanishing viscosity for traffic on networks*, SIAM Journal on Mathematical Analisys, 42(4), 1761-1783 (2010).
[25] G. Coclite, C. Donadello, *Vanishing viscosity on a star-shaped graph under general transmission conditions at the node*, Netw. Heterog. Media, 15(2), 197-213 (2020).
[26] R. Colombo, M. Garavello, *A well posed Riemann problem for the p-system at a junction*, Netw. Heterog. Media 1, No. 3, 495-511 (2006).
[27] R. Colombo, M. Herty, V. Sachers, *On 2×2 conservation laws at a junction*, SIAM Journal on Mathematical Analysis, 40, 605-622 (2008)
[28] R. Dager and E. Zuazua, *Wave Propagation, Observation and Control in 1-D Flexible Multi- Structures*, Math. Appl. 50, Springer-Verlag, Berlin, 2006.
[29] C.Dafermos, Hyperbolic Conservation Laws in Continuum Physics, Springer, Heidelberg, 2016.
[30] M. Di Francesco, P. Marcati, *Singular convergence to nonlinear diffusion waves for solutions to the Cauchy problem for the compressible Euler equations with damping*, Math. Models Methods Appl. Sci. 12, No. 9, 1317-1336 (2002).
[31] A. Gamba, D. Ambrosi, A. Coniglio, A. de Candia, S. Di Talia, E. Giraudo, G. Serini, L. Preziosi, and F. Bussolino, *Percolation, morphogenesis, and Burgers dynamics in blood vessels formation*, Phys. Rev. Lett., 90(11), 118101, 2003.
[32] M. Garavello, *A review of conservation laws on networks.*Netw. Heterog. Media 5, No.3, 565-58 (2010).
[33] M. Garavello, K. Han, B. Piccoli, Models for vehicular traffic on networks. AIMS Series on Applied Mathematics, 9. American Institute of Mathematical Sciences (AIMS), Springfield, MO, 2016.
[34] M. Garavello, R. Natalini, B. Piccoli, A. Terracina, *Conservation laws with discontinuous flux*, Netw. Heterog. Media 2, No. 1, 159-179 (2007).

[35] J. Glimm, P.D. Lax, *Decay of solutions of systems of nonlinear hyperbolic conservation laws*, Mem. Am. Math. Soc. 101, 112 p. (1970).
[36] F.R.Guarguaglini, R.Natalini, *Global smooth solutions for a hyperbolic chemotaxis model on a network*, SIAM J.Math.Anal. vol. 47, No. 6, 4652-4671 (2015).
[37] F.R.Guarguaglini, R.Natalini, *Vanishing viscosity approximation for linear transport equations on finite star-shaped networks*, J. Evol. Equ. 21, No. 2, 2413-2447 (2021).
[38] F.R. Guarguaglini, *Stationary solutions and asymptotic behaviour for a chemotaxis hyperbolic model on a network*, Netw. Heterog. Media, Vol. 13, No. 1, 47-67 (2018).
[39] F. R. Guarguaglini, *Global solutions for a chemotaxis hyperbolic-parabolic system on network with nonhomogeneous boundary conditions*, Commun. Pure Appl. Anal., vol. 19 n.2, 1057-1087 (2020).
[40] F.R. Guarguaglini, M. Papi, F. Smarrazzo, *Local and global solutions for a hyperbolic-elliptic model of chemotaxis on a network*, Math. Models Methods Appl. Sci., vol.29 n.8, 1465-1509 (2019).
[41] M. Gugat, M. Herty, and V. Schleper, *Flow control in gas networks: exact con- trollability to a given demand*, Math. Methods Appl. Sci., 34(7):745–757 (2011).
[42] A. Harten, P. Lax, B. Van Leer, *On upstream differencing and Godunov- type schemes for hyperbolic conservation laws*, SIAM Review 25 (1983), 35- 61.
[43] M. Herty, *Modeling, simulation and optimization of gas networks with compressors*, Netw. Heterog. Media 2, No. 1, 81-97 (2007).
[44] M. Herty, J. Mohring, V. Sachers, *A new model for gas flow in pipe networks*, Math. Methods Appl. Sci. 33, No. 7, 845-855 (2010).
[45] Y. Holle, M. Herty, M. Westdickenberg, *New coupling conditions for isentropic flow on networks*, Netw. Heterog. Media 15, No. 4, 605-631 (2020).
[46] S. Jin, Z. Xin, *The relaxation schemes for systems of conservation laws in arbitrary space dimensions*, Comm. Pure Appl. Math., Vol. 48, 235-277 (1995).
[47] O. Kedem, A. Katchalsky, *Thermodynamic analysis of the permeability of biological membranes to nonelectrolytes*, Biochim. Biophys. Acta 27, 229-246 (1958).
[48] P. Lefloch, M. Thanh, *The Riemann problem for fluid flows in a nozzle with discontinuous cross-section*, Commun. Math. Sci., 1, 4, 763-797 (2003).
[49] D. Maity, J.P. Raymond, A. Roy, *Existence and uniqueness of maximal strong solution of a 1D blood flow in a network of vessels*, Nonlinear Anal., Real World Appl. 63, Article ID 103405, 33 p. (2022).
[50] A. Marigo, *Entropic solutions for irrigation networks*, SIAM Journal on Applied Mathematics, 70, 1711-1735 (2010)
[51] D. Mugnolo, Semigroup methods for evolution equations on networks. Understanding Complex Systems. Springer, Cham, 2014.
[52] R. Natalini, *A discrete kinetic approximation of entropy solutions to multidimensional scalar conservation laws*,J. Differ. Equations 148, No. 2, 292-317 (1998).
[53] R. Natalini, M. Ribot, M. Twarogowska, *A well-balanced numerical scheme for a one-dimensional quasilinear hyperbolic model of chemotaxis*, Commun. Math. Sci. 12, No. 1, 13-39 (2014).
[54] R. Natalini, M. Ribot, M. Twarogowska, *A numerical comparison between degenerate parabolic and quasilinear hyperbolic models of cell movements under chemotaxis*, J. Sci. Comput. 63, No. 3, 654-677 (2015).
[55] A. Quarteroni, A. Veneziani, P. Zunino, *Mathematical and numerical modeling of solute dynamics in blood flow and arterial walls*, SIAM Journal on Numerical Analysis 39, 5, 1488-1511 (2002).
[56] A. Roggensack, *A kinetic scheme for the one-dimensional open channel flow equations with applications on networks*, Calcolo, 50, 4, 255-282 (2013)
[57] G. Serini, D. Ambrosi, E. Giraudo, A. Gamba, L. Preziosi, and F. Bussolino, *Modeling the early stages of vascular network assembly*, The EMBO J., 22(8), 1771–1779, April 2003.
[58] D. Serre, *Semi-linear and kinetic relaxation for systems of conservation laws. (Relaxations semi-linéaire et cinétique des systèmes de lois de conservation.)* Ann. Inst. Henri Poincaré, Anal. Non Linéaire 17, No. 2, 169-192 (2000).
[59] D. Serre, Systems of conservation laws 2. Geometric structures, oscillations, and initial-boundary value problems. Translated from the French by I. N. Sneddon. Cambridge: Cambridge University Press. xi, 269 p. (2000).

[60] J. Valein and E. Zuazua, *Stabilization of the wave equation on 1-D networks*, SIAM J. Control Optim., 48, 2771-2797 (2009).

Istituto per le Applicazioni del Calcolo, Consiglio Nazionale delle Ricerche
Email address: maya.briani@cnr.it

Istituto per le Applicazioni del Calcolo, Consiglio Nazionale delle Ricerche
Email address: roberto.natalini@cnr.it

Institut Denis Poisson, Université d'Orléans, CNRS, Université de Tours & Université Paris-Saclay, MaIAGE, INRAE Jouy-en-Josas
Email address: magali.ribot@univ-orleans.fr